Insights into Brain Connectivity Using Quantitative MRI Measures of White Matter

Andrew L Alexander[1] and Nancy J Lobaugh[2]

[1] Medical Physics and Psychiatry, Waisman Laboratory for Brain Imaging and Behavior, University of Wisconsin - Madison
[2] Cognitive Neurology, Sunnybrook Health Sciences Centre, University of Toronto

The vast majority of brain connectivity studies have focused on the activity of measurable brain signals in the cortex and deep gray matter nuclei regions. However, the axons in the white matter serve as the connectivity network of the brain between distant brain regions. Currently, there are not any non-invasive methods for mapping the signal conduction in specific white matter networks. Several MR imaging methods have the potential to provide information related to the physiology and pathology of the white matter tissue substrates, which may ultimately affect brain connectivity.

White matter (WM) is comprised of myelinated axons and glial cells. Axons are the thick branches of neurons, which conduct action potentials (signals) from the neuron cell body to remote target neurons. Myelin is an insulating layer of phospholipids and proteins, which significantly increase the speed of action potential conduction. Either demyelination, myelin degradation, or poor myelin development will impede the efficiency of action potentials and affect neural connectivity. The glia ("brain glue") are non-neural cells and are the supporting cells of the nervous system. They provide support, form myelin, respond to injury, maintain the blood-brain barrier, and regulate the chemical composition of tissue medium. Glial cells include oligodendrocytes (responsible for myelin generation and maintenance), astrocytes (support metabolic function and provide structural support including the blood brain barrier), and microglia (protect the brain from insult and injury). Imaging methods that can characterize the properties of this complex tissue matrix may be valuable for investigating the influence of tissue substrates on neural connectivity.

Conventional MRI is a noninvasive imaging method that can create images with exquisite anatomical detail. While standard MRI methods (e.g., T1-weighted, T2-weighted, proton-density-weighted) can differentiate gray matter and white matter, as well as localize certain brain lesions and abnormalities, it is not quantitative and does not provide information about specific changes in the tissue. However, several quantitative MRI methods have recently been developed which provide either direct or indirect measurements of relevant tissue properties including the microstructural tissue architecture, intra-myelin water, proteins associated with myelin, axon density, biochemical metabolite concentrations, and response to injury (e.g., inflammation, microglia). These MRI methods include diffusion tensor imaging, magnetization transfer imaging, T1 and T2 relaxometry, MR spectroscopy and spectroscopic imaging, and targeted contrast agents. This chapter will focus on diffusion tensor imaging (DTI), magnetization transfer imaging (MTI) and myelin water fraction imaging (MWFI) using multi-component T2 relaxometry. Although promising, MR spectroscopy is not covered here.

1 Diffusion Tensor Imaging

Diffusion tensor imaging (DTI) is currently the most widely used method for investigations of WM and anatomical connectivity. The diffusion tensor is a simple model of water diffusion in biological tissues and describes the magnitude, anisotropy (directional variation), and orientation of the diffusion distribution.

Diffusion is a random transport phenomenon, which describes the transfer of material (e.g., water molecules) from one spatial location to other locations over time. The Einstein diffusion equation (Einstein 1926):

$$\left\langle \Delta r^2 \right\rangle = 2nD\Delta t \tag{1}$$

states that the mean squared-displacement, $\langle \Delta r^2 \rangle$, from diffusion is proportional to the diffusivity, D (in mm^2/s), over the diffusion time, Δt. The displacement is scaled by the spatial dimensionality, n, which is n = 3 in biological tissues. The diffusivity of pure water at 20°C is roughly 2.0 × 10–3 mm^2/s and slightly higher at body temperature.

The molecules, sub-cellular organelles and cells within biological tissues are in a continuous state of kinetic motion. In particular, water molecules diffuse inside, outside, around, and through cellular structures. The diffusion of water molecules is first caused by random thermal fluctuations. The behavior of the diffusion is further modulated by cytoplasmic currents and the interactions with cellular membranes, and subcellular and organelles.

In fibrous tissues such as white matter tracts in the brain, water diffusion is less hindered or restricted in the direction parallel to the fiber orientation. Conversely, water diffusion is highly restricted or hindered in the directions perpendicular to the fibers. Thus, the diffusion in fibrous tissues is anisotropic. Early diffusion imaging experiments used measurements of parallel ($D_{||}$) and perpendicular ($D_\perp$) diffusion components to characterize the diffusion anisotropy (Chenevert et al. 1990; Moseley et al. 1990).

The diffusion tensor is an elegant model of water diffusion (Basser et al. 1994), which assumes that the diffusion is described by a 3D, multivariate normal distribution

$$\mathrm{P}(\Delta\vec{\mathrm{r}}, \Delta \mathrm{t}) = \frac{1}{\sqrt{(4\pi\Delta \mathrm{t})^3|\mathbf{D}|}} exp\left\{\frac{-\Delta\vec{\mathrm{r}}^{\mathrm{T}}\mathbf{D}^{-1}\Delta\vec{\mathrm{r}}}{4\Delta \mathrm{t}}\right\} \tag{2}$$

where Δr is the displacement vector, Δt is the diffusion time, and D is the diffusion tensor, which is a 3×3 matrix

$$\mathbf{D} = \begin{bmatrix} D_{xx} & D_{xy} & D_{xz} \\ D_{yx} & D_{yy} & D_{yz} \\ D_{zx} & D_{zy} & D_{zz} \end{bmatrix}. \tag{3}$$

The diffusion tensor may be diagonalized to calculate the eigenvalues $(\lambda_1,\ \lambda_2,\ \lambda_3)$ and corresponding eigenvectors $(\hat{e}_1, \hat{e}_2, \hat{e}_3)$ of the diffusion tensor, which describe the relative amplitudes of diffusion and the directions of the principle diffusion axes. A common visual representation of the diffusion tensor is an ellipsoid with the principal axes aligned with the eigenvectors and axes lengths a function of the eigenvalues (see Fig. 1). In the case where the diffusion eigenvalues are (roughly) equal (e.g., $\lambda_1 \sim \lambda_2 \sim \lambda_3$), the diffusion tensor is (nearly) isotropic. When the eigenvalues are significantly different in magnitude (e.g., $\lambda_1 > \lambda_2 > \lambda_3$), the diffusion tensor is anisotropic. Changes in local tissue microstructure with many types of tissue injury, disease or normal physiological changes (i.e., aging) will cause changes in the eigenvalue magnitudes. Thus, the diffusion tensor is an extremely sensitive probe for characterizing both normal and abnormal tissue microstructure.

More specifically in the CNS, water diffusion is typically anisotropic in white matter regions, and isotropic in both gray matter and cerebrospinal fluid (CSF). The major diffusion eigenvector ($\hat{e}_1$-direction of greatest diffusivity) is assumed to be parallel to the tract orientation in regions of homogenous white matter. This directional relationship is the basis for estimating the trajectories of white matter pathways with tractography algorithms.

Diffusion-Weighted Image Acquisition

The random motion of water molecules in biological tissues may cause the signal intensity to decrease in MRI. The NMR signal attenuation from molecular

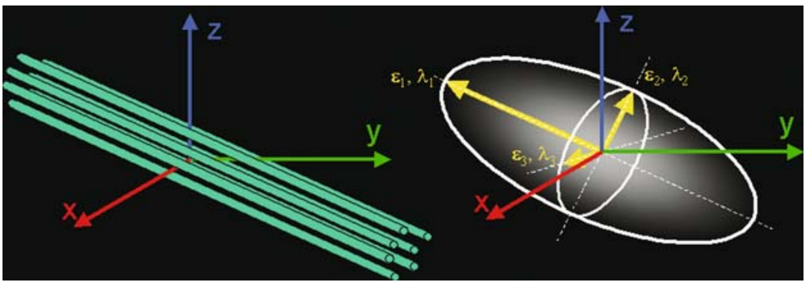

Fig. 1. Schematic representations of diffusion displacement distributions for the diffusion tensor. Ellipsoids (*right*) are used to represent diffusion displacements. The diffusion is highly anisotropic in fibrous tissues such as white matter (*left*). The direction of greatest diffusivity is generally assumed to be parallel to the local direction of white matter

diffusion was first observed more than a half century ago by Hahn (1950). Subsequently, Stejskal & Tanner (1965) described the NMR signal attenuation in the presence of field gradients. More recently, field gradient pulses have been used to create diffusion-weighted MR images (Le Bihan 1990).

Typically, the diffusion weighting is performed using two gradient pulses with equal magnitude and duration (Fig. 2). The first gradient pulse dephases the magnetization across the sample (or voxel in imaging); and the second pulse rephases the magnetization. For stationary (non-diffusing) molecules, the phases induced by both gradient pulses will completely cancel, the magnetization will be maximally coherent, and there will be no signal attenuation from diffusion. In the case of coherent flow in the direction of the applied gradient, the bulk motion will cause the signal phase to change by different amounts for each pulse so that there will be a net phase difference, $\Delta\phi = \gamma v G \delta \Delta$, which is proportional to the velocity, v, the area of the gradient pulses defined by the amplitude, G, and the duration, δ, and the spacing between the pulses, Δ. The gyromagnetic ratio is γ. This is also the basis for phase contrast angiography. For the case of diffusion, the water molecules are also moving, but in arbitrary directions and with variable effective velocities. Thus, in the presence of diffusion gradients, each diffusing molecule will accumulate a different amount of phase. The diffusion-weighted signal is created by summing the magnetization from all water molecules in a voxel. The phase dispersion from diffusion will cause destructive interference, which will cause signal attenuation. For simple isotropic Gaussian diffusion, the signal attenuation for the diffusion gradient pulses in Fig. 2 is described by

$$S = S_o \, e^{-bD} \tag{4}$$

where S is the diffusion-weighted signal, S_o is the signal without any diffusion-weighting gradients (but otherwise identical imaging parameters), D is the apparent diffusion coefficient, and b is the diffusion weighting described by the properties of the pulse pair:

$$b = (\gamma G \delta)^2 (\Delta - \delta/3) \tag{5}$$

Diffusion weighting may be achieved using either a bipolar gradient pulse pair or identical gradient pulses that bracket a 180° refocusing pulse as shown in Fig. 2.

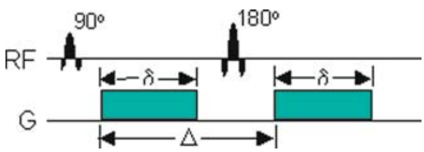

Fig. 2. Spin echo pulse sequence scheme for pulsed-gradient diffusion weighting. A spin-echo refocusing pulse (180°) causes the gradient pulses to be diffusion-weighted

The large gradients make DW MRI extremely sensitive to subject motion. Very small amounts of subject motion may lead to phase inconsistencies in the raw k-space data, causing severe ghosting artifacts in the reconstructed images. Recently, the advances in gradient hardware (maximum gradient amplitude and speed) and the availability of echo planar imaging (EPI) (Mansfield 1984; Turner et al. 1990) on clinical MRI scanners have made routine DW-MRI studies possible. A schematic of a DW-EPI pulse sequence is shown in Fig. 3. With EPI, the image data for a single slice may be collected in 100ms or less, effectively "freezing" any head motion. The fast acquisition speed of EPI makes it highly efficient, which is important for maximizing the image signal-to-noise ratio (SNR) and the accuracy of the diffusion measurements. Thus, single-shot EPI is the most common acquisition method for diffusion-weighted imaging. However, the disadvantages of single shot EPI can also be significant. First, both magnetic field inhomogeneities (Jezzard and Balaban 1995) and eddy currents (Haselgrove and Moore 1996) can warp the image data, thereby compromising the spatial fidelity. Distortions from eddy currents may be either minimized using bipolar diffusion gradient encoding schemes (Alexander et al. 1997; Reese et al. 2003), or corrected retrospectively using image co-registration methods (Haselgrove and Moore 1996; Andersson and Skare 2002; Rohde et al. 2004). Distortions from static field inhomogeneities may be either reduced by using parallel imaging methods such as SENSE (Pruessmann et al. 1999) or retrospectively corrected using maps of the magnetic field (Jezzard and Balaban 1995). Misalignments of k-space data on odd and even lines of k-space will lead to Nyquist or half-field ghosts in the image data. In general, the system should be calibrated to minimize this ghosting although post-processing correction methods have been developed (Zhang and Wehrli 2004). The spatial resolution of 2D EPI pulse sequences also tends

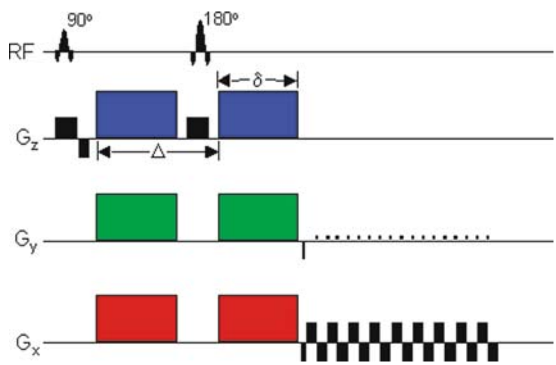

Fig. 3. Schematic of a DW EPI pulse sequence. A spin echo pulse is used to achieve diffusion-weighting from the gradient pulse pairs (colored) as illustrated in Fig. 5. The imaging gradients are shown in black. Diffusion-weighting gradients can be applied in any arbitrary direction using combinations of G_x (*red*), G_y (*green*) and G_z (*blue*)

to be limited. At 1.5T, it is possible to acquire 2.5 mm isotropic voxels over the entire brain in roughly 15 minutes (Jones et al. 2002b). Smaller voxel dimensions may be achieved using either more sensitive RF coils or by going to higher field strengths. Alternative DW imaging techniques, such as PROPELLER (Pipe et al. 2002) and line scan (Gudbjartsson et al. 1997), are less sensitive to motion, eddy currents and B0 distortions.

In the case of anisotropic diffusion, the direction of the diffusion encoding will influence the amount of attenuation. The cartoon in Fig. 4 illustrates the basis for diffusion anisotropy contrast. For anisotropic tissues like white matter, when the diffusion encoding directions are applied parallel to the white matter tract, the signal is highly attenuated. However, when the encoding direction is applied perpendicular to the tract, the diffusion is significantly hindered and the attenuation is much less than in the parallel case. In more isotropic structure regions (such as gray matter), the signal attenuation is independent of the encoding direction.

A minimum of six non-collinear diffusion encoded measurements are necessary to measure the full diffusion tensor (Shrager and Basser 1998; Papadakis et al. 1999). A wide variety of diffusion-tensor encoding strategies with six or more encoding directions have been proposed (e.g., Basser and Pierpaoli 1998; Jones et al. 1999; Papadakis et al. 1999; Shimony et al. 1999; Hasan et al. 2001b). An example of images with DW encoding in twelve directions

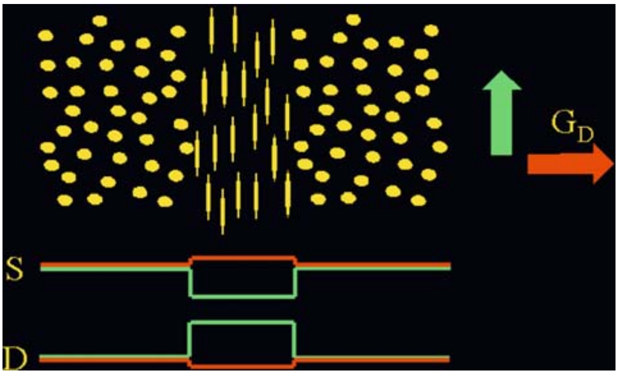

Fig. 4. Illustration of anisotropic signal attenuation with diffusion encoding direction. When the diffusion-weighting (G_D) is applied in the direction parallel (*green*) to the anisotropic cellular structures (e.g., white matter), the signal (S) is strongly attenuated and the apparent diffusivity (D) is high. Conversely, when the diffusion-weighting is applied in the direction perpendicular to the fibrous tissue, the diffusion is less attenuated and the apparent diffusivity is lower. The signal attenuation and diffusivities are independent of the encoding direction in the anisotropic tissue regions. The difference in the directional diffusivities is the source of anisotropy contrast in DTI. The direction of diffusion encoding is selected using different combinations of the diffusion gradients in G_x, G_y and G_z

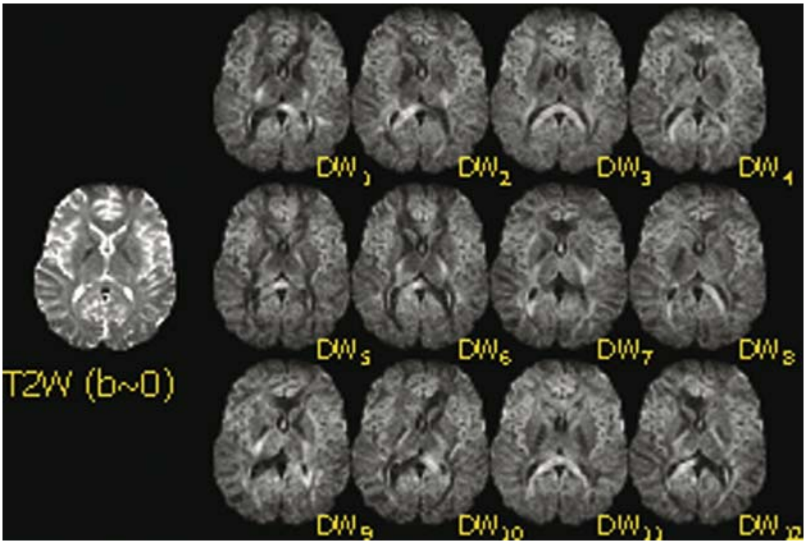

Fig. 5. Example images from a DTI study for a single slice in a human brain. The image on the left is without any diffusion-weighting and is T2-weighted. The twelve images on the right were obtained with diffusion weighting (b = 1000 s/mm^2) applied in twelve non-collinear directions. Note that the image contrast changes significantly with the diffusion encoding direction

for a single slice is shown in Fig. 5. The observed contrast difference for each of the 12 DW encoded images is the basis for the measurement of diffusion anisotropy, which is described later. The selection of tensor encoding directions is critical for accurate and unbiased assessment of diffusion tensor measures. Hasan et al. (2001b) performed a comprehensive comparison of various heuristic, numerically optimized and natural polyhedra encoding sets. This study demonstrated that encoding sets with uniform angular sampling yield the most accurate diffusion tensor estimates. Several recent studies have provided mounting evidence that more diffusion encoding directions causes the measurement errors to be independent of the tensor orientation (e.g., Batchelor et al. 2003; Jones 2004).

There are a number of considerations that should be made when prescribing a diffusion tensor protocol. This is moderately complicated by the wide spectrum of pulse sequence parameters that must be configured. As discussed above, diffusion-weighted, spin-echo, single-shot EPI is the most common pulse sequence for DTI. The optimum diffusion-weighting (also called b-value) for the brain is roughly between 700 and 1300 s/mm^2 with a b-value of 1000 s/mm^2 being most common. The selection of the number of encoding directions is dependent upon the availability of encoding direction sets, the desired scan time and the maximum number of images that can be obtained in a series. Measurements of diffusion anisotropy tend to be quite sensitive to image noise, which can also lead to biases in the anisotropy estimates (overestimation of major eigenvalue; underestimation of minor eigenvalue; increase in uncertainty of all eigenvalues) (Pierpaoli and Basser 1996; Chang et al. 2005; Rohde et al. 2005). The accuracy of DTI measures may be improved by either increasing the number of encoding directions or increasing the number of averages. Additional procedures proposed to reduce artifact include the use of peripheral gating to minimize motion related to cardiac pulsitility (Skare and Andersson 2001) and inversion-recovery pulses to minimize partial volume effects from CSF (Bastin 2001; Papadakis et al. 2002; Concha et al. 2005b). Unfortunately, these procedures typically increase the scan time for DTI data collection, and can reduce SNR. The image SNR can also obviously be improved by using larger voxels, although this will increase partial volume averaging of tissues, which can lead to errors in the fits to the diffusion tensor model (Alexander et al. 2001a). The specific parameters for a protocol will depend upon the application. For many routine clinical applications (brain screening, stroke, brain tumors), a fairly coarse spatial resolution can be used with a small number of encoding directions. However, for applications requiring accurate quantification (i.e., quantifying DTI measures in very small white matter tracts, or estimating white matter trajectories with white matter tractography) high spatial resolution is much more important and a large number of diffusion encoding directions or averaging is desirable. High quality DTI data with whole brain coverage, 2.5 mm isotropic resolution and 64 diffusion encoding directions may be obtained in approximately 15 minutes on clinical 1.5T scanners (Jones et al. 2002b). Similar DTI data quality can be achieved in half the time or less at 3.0T, except the image distortions are roughly double.

Diffusion Tensor Image Processing

Maps of DTI measures (mean diffusivity, anisotropy, orientation) are estimated from the raw DW images. As discussed previously, the images may be distorted and misregistered from a combination of eddy currents, subject motion, and magnetic field inhomogeneities. Ideally, these distortions and sources of misregistration should be corrected before calculating any subsequent quantitative diffusion maps. In cases where corrections are not restricted to in-plane errors and distortions, this correction should include recalculation of the diffusion gradient directions or reorienting the tensors (Alexander et al. 2001b; Andersson and Skare 2002; Rohde et al. 2004).

The first step in estimating the diffusion tensor and the associated measures is to calculate the apparent diffusivity maps, $D_{i,app}$, for each encoding direction. The signal attenuation for scalar or isotropic diffusion is described in (4). However, this equation has to be adjusted to describe the signal attenuation for anisotropic diffusion with the diffusion tensor:

$$S_i = S_o\ e^{-b\hat{g}_i^T \mathbf{D} \hat{g}_i} = S_o\ e^{-bD_{i,app}} \tag{6}$$

where S_i is the DW signal in the ith encoding direction, $\hat{g}_i$ is the unit vector describing the DW encoding direction, and b is the amount of diffusion weighting in (6). The apparent diffusivity maps are generated by taking the natural log of (6) and solving for $D_{i,app}$:

$$D_{i,app} = \frac{ln(S_i) - ln(S_o)}{b} \tag{7}$$

This equation works when measurements are obtained for a single diffusion-weighting (b-value) and an image with very little or no diffusion-weighting (S_o). The six independent elements of the diffusion tensor (D_{xx}, D_{yy}, D_{zz}, $D_{xy} = D_{yx}$, $D_{xz} = D_{zx}$, and $D_{yz} = D_{zy}$) may be estimated from the apparent diffusivities using least squares methods (Basser et al. 1994; Hasan et al. 2001a). Maps of the diffusion tensor elements for the data in Fig. 5 are shown in Fig. 6.

Diffusion Tensor Image Measures

The display, meaningful measurement, and interpretation of 3D image data with a 3 × 3 diffusion matrix at each voxel is a challenging task without simplification of the data. Consequently, it is desirable to distill the image information into simpler scalar maps, particularly for routine clinical applications. The two most common measures are the trace and anisotropy of the

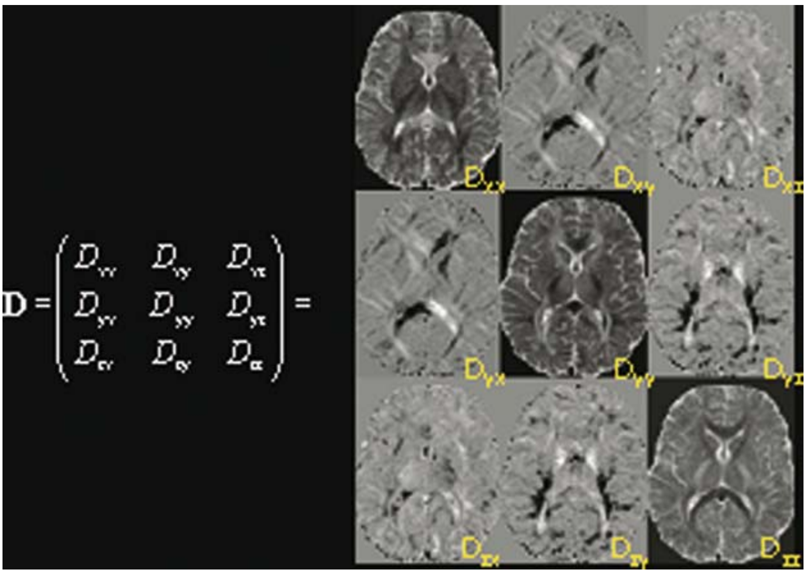

Fig. 6. Maps of the diffusion tensor elements for the DTI data in Fig. 5. Note that the off-diagonal images are symmetric about the diagonal and that the values are both positive and negative

diffusion tensor. The trace of the tensor (Tr), or sum of the diagonal elements of D, is a measure of the magnitude of diffusion and is rotationally invariant. The mean diffusivity, MD, (also called the apparent diffusion coefficient or ADC) is used in many published studies and is simply the trace divided by three (MD = Tr/3). The degree to which the signal is a function of the DW encoding direction is represented by measures of tensor anisotropy. Many measures of anisotropy have been described (Basser and Pierpaoli 1996; Conturo et al. 1996; Pierpaoli and Basser 1996; Ulug and van Zijl 1999; Westin et al. 2002) Most of these measures are rotationally invariant, but do have differential sensitivity to noise (e.g., Skare et al. 2000). Currently, the most widely used invariant measure of anisotropy is the Fractional Anisotropy (FA) described originally by Basser & Pierpaoli (1996).

$$\mathrm{FA} = \sqrt{\frac{(\lambda_1 - \mathrm{MD})^2 + (\lambda_2 - \mathrm{MD})^2 + (\lambda_3 - \mathrm{MD})^2}{2({\lambda_1}^2 + {\lambda_2}^2 + {\lambda_3}^2)}} \tag{8}$$

A third important measure is the tensor orientation described by the major eigenvector direction. For diffusion tensors with high anisotropy, the major eigenvector direction is generally assumed to be parallel to the direction of white matter tract, which is often represented using an RGB (red-green-blue) color map to indicate the eigenvector orientations (Makris et al. 1997; Pajevic and Pierpaoli 1999). The local eigenvector orientations can be used to identify and parcellate specific WM tracts; thus DT-MRI has an excellent potential for applications that require high anatomical specificity. The ability to identify specific white matter tracts on the eigenvector color maps has proven useful for mapping white matter anatomy relative to lesions for preoperative planning (Witwer et al. 2002) and post-operative follow-up (Field et al. 2004). Recently, statistical methods have been developed for quantifying the distributions of tensor orientation in specific brain regions (Wu et al. 2004). Example maps of the mean diffusivity, fractional anisotropy, and major eigenvector direction are shown in Fig. 7.

Relationship to White Matter Physiology & Pathology

The applications of DTI are rapidly growing, in part because the diffusion tensor is exquisitely sensitive to subtle changes or differences in tissue at the microstructural level. DTI studies have found differences in development (e.g., Barnea-Goraly et al. 2005; Snook et al. 2005) and aging (e.g., Abe et al. 2002; Pfefferbaum et al. 2005; Salat et al. 2005), and across a broad spectrum of diseases and disorders including traumatic brain injury (diffuse axonal injury) (Werring et al. 1998; Salmond et al. 2006), epilepsy (Concha et al. 2005a), multiple sclerosis (Cercignani et al. 2000; Rovaris et al. 2002; Assaf et al. 2005), ALS (Ellis et al. 1999; Jacob et al. 2003; Toosy et al. 2003), schizophrenia (Buchsbaum et al. 1998; Lim et al. 1999; Agartz et al. 2001; Jones et al. 2006), bipolar disorder (Adler et al. 2004; Beyer et al. 2005), OCD

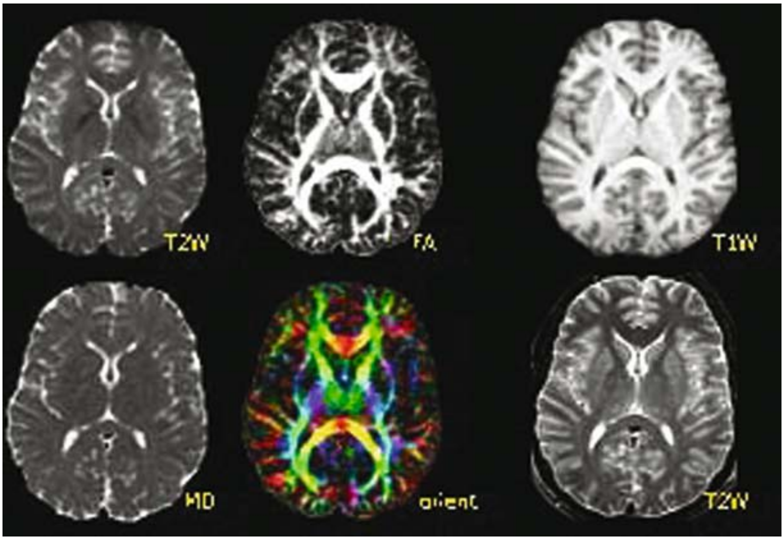

Fig. 7. DTI maps computed from data in Figs. 5 and 6. The images are (*top-left*): T2-weighted "reference" (or b = 0) image from DTI data; (*bottom-left*): mean diffusivity (note similar contrast to T2-W image with CSF appearing hyperintense); (*top-middle*): fractional anisotropy (hyperintense in white matter); (*bottom-middle*) major eigenvector direction indicated by color (red = R/L, green = A/P, blue = S/I) weighted by the FA (note that specific tract groups can be readily identified). Conventional T1-weighted and T2-weighted images (*right column*) at the same anatomical location are shown

(Szeszko et al. 2005), autism (Barnea-Goraly et al. 2004), HIV-AIDs (Pomara et al. 2001; Ragin et al. 2004), and Fragile X (Barnea-Goraly et al. 2003). In nearly all cases, diffusion anisotropy (e.g., fractional anisotropy – FA) is decreased and diffusivity increased in affected regions of diseased white matter relative to healthy controls, while the reverse is true for healthy white matter in development (FA increases, diffusivity decreases).

It is important to note that diffusion anisotropy does not describe the full tensor shape or distribution. This is because different eigenvalue combinations can generate the same values of FA (Alexander et al. 2000). So, for example, a decrease in FA may reflect a decreased major (largest) eigenvalue and/or increased medium/minor (smallest) eigenvalues. FA is likely to be adequate for many applications and appears to be quite sensitive to a broad spectrum of pathological conditions. However, changes simply indicate some difference exists in the tissue microstructure. Several recent studies have looked more directly at the diffusion eigenvalues to determine if they can provide more specific information about the microstructural differences. The results have suggested that the eigenvalue amplitudes or combinations of the eigenvalues (e.g., the radial diffusivity, $D_r = (\lambda_2 + \lambda_3)/2$) demonstrate specific relationships to white matter pathology. For example, the radial diffusivity appears to be specific to myelination in white matter (Song et al. 2005), whereas the axial diffusivity ($D_a = \lambda_1$) is more specific to axonal density, making it a good model of axonal degeneration (Song et al. 2002). Tensor shape can be fully described using a combination of spherical, linear and planar shape measures (Alexander et al. 2000; Westin et al. 2002), which may also be useful for understanding WM pathology. Consequently, it is important to consider alternative quantitative methods when trying to interpret DTI measurements.

Beyond the Diffusion Tensor

The diffusion tensor is a good model of the diffusion-weighted signal behavior for low levels of diffusion weighting (e.g., $b < 1500\,\mathrm{s/mm^2}$). However, the diffusion tensor model does not appear to be consistently accurate in describing the signal behavior for higher levels of diffusion-weighting (e.g., $b > 2000\,\mathrm{s/mm^2}$). The problems with the simple diffusion tensor model arise from two sources – (1) apparent "fast" and "slow" diffusing components (Mulkern et al. 1999) that cause the signal decay with diffusion-weighting to appear bi-exponential; and (2) partial volume averaging (e.g.,Alexander et al. 2001a) between tissue groups with distinct diffusion tensor properties (e.g., crossing white matter (WM) tracts, averaging between WM and gray matter tissues). The fast and slow diffusion signals are likely to arise from local restriction effects from cellular membranes although some have hypothesized that these signals correspond to intra- and extra-cellular diffusion.

The effect of partial volume averaging causes ambiguities in the interpretation of diffusion tensor measurements. Whereas the diffusion anisotropy is generally assumed to be high in white matter, regions of crossing white matter tracts will have artifactually low diffusion anisotropy. Consequently, in regions with complex white matter organization, changes or differences in diffusion tensor measures may reflect changes in either the tissue microstructure or the partial volume averaging components. As the diffusion-weighting is increased, the profiles of apparent diffusivity reveal non-Gaussian diffusion behavior in voxels with partial volume averaging.

A growing number of strategies have been developed for measuring and interpreting complex diffusion behavior. The methods vary in their acquisition sampling and analysis approaches. For all of the approaches described here, increasing the maximum diffusion-weighting will improve the characterization of both the slow diffusion components and the partial volume effects, although the measurement SNR will be decreased.

Fast/Slow Diffusion Modeling: Diffusion-weighted measurements over a range of diffusion-weighting have been used to estimate apparent fast and slow components of both apparent diffusivities (BEDI: bi-exponential diffusion imaging) and diffusion tensors (MDTI: multiple diffusion tensor imaging) (Niendorf et al. 1996; Mulkern et al. 1999; Maier et al. 2004). In these cases, the measurements are fit to:

$$S = S_o\left((k)\,e^{-b\hat{g}^T\mathbf{D}_f\hat{g}} + (1-k)\,e^{-b\hat{g}^T\mathbf{D}_s\hat{g}}\right) \tag{9}$$

where $\mathbf{D}_f$ and $\mathbf{D}_s$ are the fast and slow diffusion tensors, and k is the signal fraction from the fast compartment. For a fixed diffusion encoding direction, the signal decay appears bi-exponential with diffusion-weighting. Bi-exponential strategies are appropriate for the cases where there is no significant partial voluming expected and when the diffusion may be modeled using a combination of narrow and broad Gaussian distributions. As discussed earlier, partial volume effects (e.g., crossing WM fibers) will significantly complicate the interpretation of fast and slow diffusing components. In addition, the assignment of these components has been controversial.

High Angular Resolution Diffusion Imaging (HARDI): In order to better characterize the angular diffusion features associated with crossing white matter tracts, several diffusion encoding approaches have been developed that use a large number of encoding directions ($N_e > 40$ up to several hundred) at a fixed level of diffusion-weighting(Alexander et al. 2002; Frank 2002). Although HARDI studies have been reported with diffusion-weighting as low as $b = 1000\,\mathrm{s/mm}^2$ (Alexander et al. 2002), the separation of tract components will be much better for higher diffusion-weighting. The original HARDI methods estimated the profiles of apparent diffusion coefficients and used spherical harmonic decomposition methods to estimate the complexity of the diffusion profiles (Alexander et al. 2002; Frank 2002).

Higher order spherical harmonic basis functions represent signal terms that may correspond to crossing white matter tracts in the voxel. Odd spherical harmonic orders do not correspond to meaningful diffusion measurements and are generally assumed to be noise and artifacts.

The HARDI 3D diffusion profiles may also be modeled using generalized diffusion tensor imaging (GDTI) (Ozarslan and Mareci 2003; Liu et al. 2004) which use higher order tensor statistics to model the ADC profile. The GDTI methods proposed by Liu et al. (2004) demonstrate the impressive ability to model asymmetrically bounded diffusion behavior, although the method requires the accurate measurement of the signal phase, which is nearly always discarded and may be difficult to obtain in practice. One problem with these approaches is that in the case of crossing white matter tracts, the directions of maximum ADC do not necessarily correspond to the fiber directions.

One approach to this problem is the q-ball imaging (QBI) solution described by Tuch (2004), which estimates the orientational distribution function (ODF) based upon the Funk-Radon Transform. According to this relationship, the ODF for a particular direction is equivalent to the circular integral about the equator perpendicular to the direction

$$\mathrm{ODF}(\hat{\mathrm{r}}) = \int\int\int_{\mathrm{q}\perp\hat{\mathrm{r}}} \mathrm{E}(\mathbf{q}, \Delta)\mathrm{d}^3\mathbf{q} \tag{10}$$

This integral requires that the diffusivities be interpolated over the entire surface of the sphere. Whereas the peaks in the HARDI profile do not necessarily conform to the WM tract directions (see Fig. 8), the peaks in the ODF profiles do in fact correspond to the specific WM tract direction. Since the ODF is

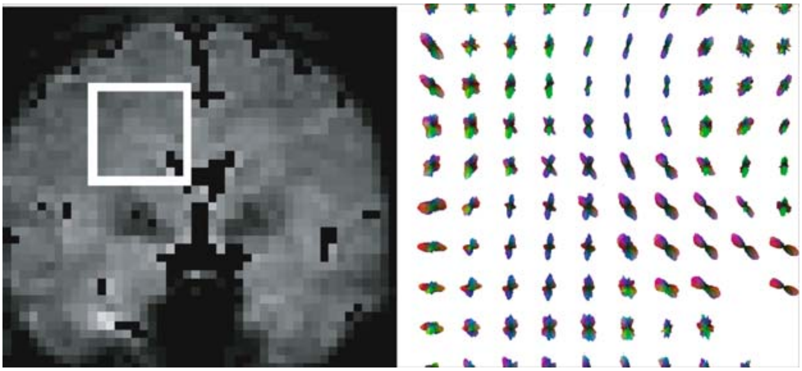

Fig. 8. Example QBI orientational density function (ODF) map for region at the intersection of the corpus callosum, corona radiata and superior longitudinal fasciculus. Regions of crossing WM tracts are clearly observed

estimated by integrating several measurements together, the SNR of the ODF will be much higher than that of the ADC values in the original HARDI.

Diffusion Spectrum Imaging (DSI): The fast/slow diffusion modeling and HARDI approaches represent opposing approaches to complex diffusion characterization. The combination of high angular sampling at multiple levels of diffusion weighting may be used to provide information about both fast/slow diffusion and crossing WM tract orientations. The most basic approach for this application is diffusion spectrum imaging (DSI) (Wedeen et al. 2005) which uses diffusion-weighted samples on a Cartesian q-space lattice, where $\mathbf{q} = \gamma\mathbf{G}\delta$ is the diffusion-weighting wave-vector analogous to wave-vector $\mathbf{k}$ used in k-space sampling for MR image acquisitions. An excellent discussion of q-space imaging is found in the text by Callaghan (1994). For a specified diffusion time, Δ, the probability distribution of diffusion displacements, $\mathrm{P}(\mathbf{R}, \Delta)$, is related to the distribution of sampled diffusion-weighted signals in q-space, $\mathrm{E}(\mathbf{q}, \Delta)$, through a Fourier Transform:

$$\mathrm{P}(\mathbf{R}, \Delta) = \int\int\int \mathrm{E}(\mathbf{q}, \Delta)\mathrm{e}^{-\mathrm{i}2\pi\mathbf{q}\cdot\mathbf{R}}\mathrm{d}^3\mathbf{q} \tag{11}$$

The derivations of q-space formalism assume that the widths of the diffusion-pulses, δ, are narrow relative to the pulse spacing, Δ, such that $\delta << \Delta$. The maximum gradient amplitudes on current clinical MRI systems cause this assumption to be violated for diffusion spectrum imaging, since $\delta \sim \Delta$. The effect of this will be to slightly, but consistently underestimate the diffusion displacements, but the overall distribution shape will be correct (Wedeen et al. 2005). Note that relationship of DSI (q-space) to diffusion tensor imaging is that $\mathrm{P}(\mathbf{R}, \Delta)$ is a multivariate Gaussian and the diffusion-weighting factor is $\mathrm{b} = |\mathrm{q}|^2(\Delta - \delta/3)$ or $\mathrm{b} \sim |\mathrm{q}|^2\Delta$ for small δ. The DSI approach yields empirical estimates of the distributions of diffusion displacements (e.g., model free), which are described using the standard definitions of Fourier sampling theory.

Since the distributions of diffusion displacements are model independent, the distributions may be challenging to quantify. Several features have been proposed including the zero-displacement probability, $P(\mathbf{R} = 0, \Delta)$, which is higher in regions with more hindered or restricted diffusion; the mean squared displacement,

$$\mathrm{MSD}(\Delta) = \int\int\int P(\mathbf{R}, \Delta)|R|^2 \, d^3\mathbf{R} \tag{12}$$

which is related to the diffusivity (see Fig. 9); the kurtosis of the diffusion distribution, which highlights regions of significant slow diffusion; and the orientational distribution function (ODF)(Wedeen et al. 2005):

$$\mathrm{ODF}(\hat{r}) = \int P(R\hat{r}, \Delta)|R|^2 \, dR \tag{13}$$

Note that this definition of ODF (Eq (9)) for DSI is derived differently for DSI than it is for QBI (Tuch 2004).

While Cartesian sampling facilitates the straightforward FFT for estimation of the displacement densities, Cartesian sampling is not required. Recently, investigators have proposed non-Cartesian sampling strategies of q-space including sampling on concentric spherical shells of constant $|q|$ (Assaf et al. 2004; Wu and Alexander 2005). Assaf et al. then applied a model (CHARMED) of slow and fast diffusing compartments to estimate what they deemed as hindered and restricted diffusion (Assaf et al. 2004). Wu and

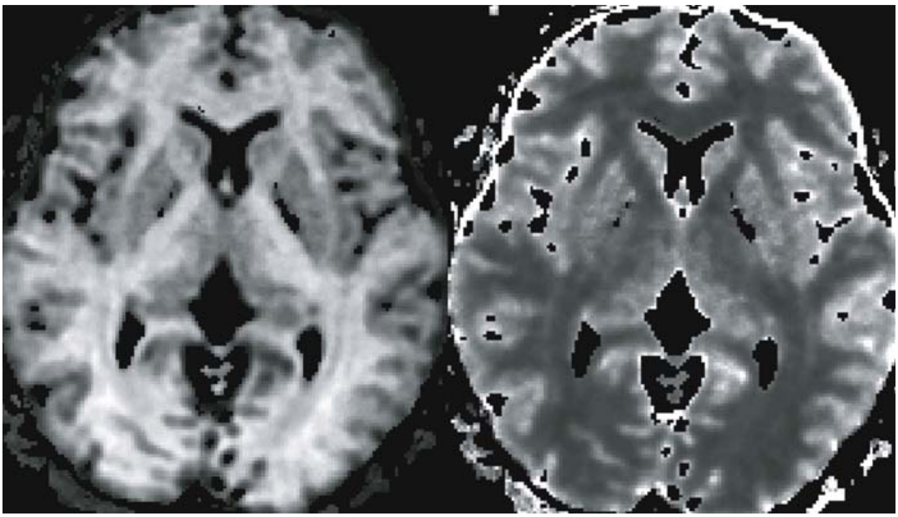

Fig. 9. Example $P(\mathbf{R} = 0;\ \Delta)$ and mean squared displacement maps from DSI study ($N_e = 257;\ \mathrm{bmax} = 9000\,\mathrm{s/mm^2}$)

Alexander (2005) demonstrated that the concentric q-space shell samples in hybrid diffusion imaging (HYDI) could be used for DTI, DSI and QBI in the same experiment.

Applications of High Diffusion-Weighting: The complexity and time required to perform advanced diffusion imaging methods with high diffusion-weighting has limited the number of clinical and research studies relative to the work in diffusion tensor imaging. The pathophysiologic significance of fast/slow diffusion measurements is unclear. Only one published study to date (Brugieres et al. 2004) has specifically examined the effects of pathology (ischemia) on the fast and slow diffusion components. Several small studies of hybrid DSI methods have shown promise in being sensitive to white matter changes associated with multiple sclerosis (Assaf et al. 2002a; Cohen and Assaf 2002), autoimmune neuritis (Assaf et al. 2002b), and vascular dementia (Assaf et al. 2002c). Clearly, more studies are necessary to justify longer imaging times than DTI. To date, none of these methods have been used to directly investigate the relationships to brain connectivity.

From Diffusion to Pathways: White Matter Tractography

In addition to providing information about the mean diffusivity and anisotropy, diffusion imaging methods can also yield novel information about the orientation of local anisotropic tissue features such as bundles of white matter fascicles. In diffusion tensor imaging, the direction of the major eigenvector, $\mathbf{e}_1$, is generally assumed to be parallel to the direction of white matter. This directional information can be visualized by breaking down the major eigenvector into x, y and z components, which can be represented using RGB colors – e.g., Red = e_{1x} =Right/Left; Green= e_{1y} =Anterior/Posterior; Blue= e_{1z} =Inferior/Superior. Maps of WM tract direction can be generated by weighting the RGB color map by an anisotropy measure such as FA (Pajevic and Pierpaoli 1999). For many applications, the use of color labeling is useful for identifying specific WM tracts and visualizing their rough trajectories. An alternative strategy is white matter tractography (WMT), which uses the directional information from diffusion measurements to estimate the trajectories of the white matter pathways. WMT increases the specificity of WM pathway estimates and enables the 3D visualization of these trajectories, which may be challenging using cross-sectional RGB maps.

Deterministic Tractography Algorithms: Most WMT algorithms estimate trajectories from a set of "seed" points. Generally, WMT algorithms may be divided into two classes of algorithms – deterministic (e.g., streamline) and probabilistic (see below). Streamline algorithms are based upon the equation:

$$d\mathbf{r} = \mathbf{v}_{\text{traj}} d\tau \tag{14}$$

where $\mathbf{r}(\tau)$ is the path and $\mathbf{v}_{\text{traj}}$ is the vector field that defines the local path direction. Typically, streamline WMT algorithms use major eigenvector field to define the local trajectory directions $\mathbf{v}_{\mathrm{traj}} = \mathbf{e}_1$ at each step (Conturo et al. 1999; Mori et al. 1999; Basser et al. 2000) (see Fig. 10). Alternatively, tensor deflection (TEND) $\mathbf{v}_{\mathrm{traj}} = \mathbf{D}\cdot\mathbf{v}_{\mathrm{in}}$ uses the entire diffusion tensor to define the local trajectory direction (Lazar et al. 2003). The integration of deterministic pathways may be performed using simple step-wise algorithms including FACT (Mori et al. 1999) and Euler (e.g., $\Delta\mathbf{r} = \mathbf{v}_{\mathrm{traj}}\,\Delta\tau$) (Conturo et al. 1999) integration, or more continuous integration methods such as 2$^{\mathrm{nd}}$ or 4$^{\mathrm{th}}$ order Runge-Kutta (Basser et al. 2000), which enable more accurate estimates of curved tracts.

Deterministic Tractography Errors: WMT can be visually stunning (see Fig. 11). However, one significant limitation with WMT is that the errors in an estimated tract are generally unknown. Further, the visual aesthetic of WMT, which look like actual white matter patterns, can potentially instill a false sense of confidence in specific results. Unfortunately, there are many potential sources of error that can confound WMT results. Very small perturbations in the image data (i.e., noise, distortion, ghosting, etc.) may lead to significant errors in a complex tensor field such as the brain. Recent studies

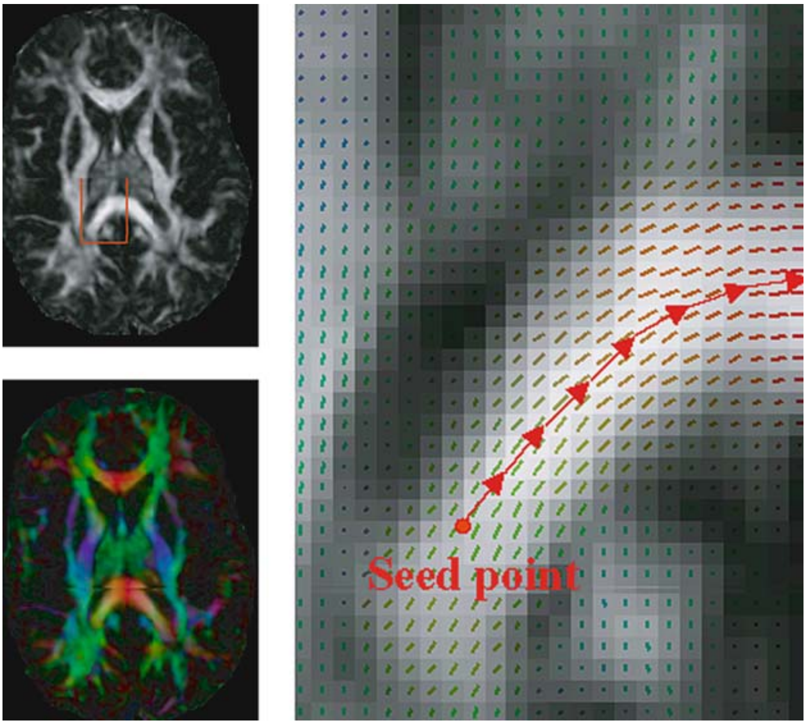

Fig. 10. FA and $\mathbf{e_1}$ color map depicting WM tract orientation. The principle concept of streamline WMT is depicted in a region of corpus callosum. The trajectory is started from a single seed point and the path estimated at discrete steps

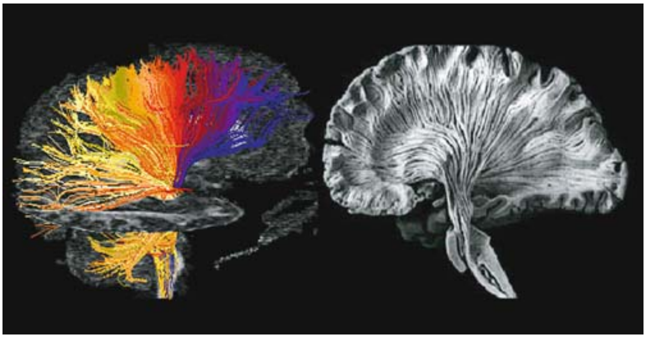

Fig. 11. WMT (*left*) appears to be very similar to an actual white matter dissection (*right*) (Virtual Hospital). http://web.archive.org/web/20050407073533/www.vh.org/adult/provider/anatomy/BrainAnatomy/BrainAnatomy.html

have shown that the dispersion in tract estimates $< \Delta x^2 >$ from image noise is roughly proportional to the distance (N·w, where N is the number of voxels and w is voxel size) and inversely proportional to the squares of the eigenvalue differences ($\Delta\lambda_j = \lambda_1 - \lambda_j$) and SNR (Anderson 2001; Lazar et al. 2003)

$$< \Delta x_j{}^2 >= N \cdot w^2 \cdot E/(\Delta\lambda_j \cdot SNR)^2 \tag{15}$$

where E is a factor related to the diffusion tensor encoding scheme and the diffusion tensor orientation, and $j = 2, 3$. Further, the tract dispersion is also affected by the local divergence of the tensor field (Lazar et al. 2003). Even in the complete absence of noise and image artifacts, most current deterministic methods cannot accurately map WM pathways in regions with crossing or converging fibers, which has led to the development of visualization tools to highlight these regions of uncertainty (Jones 2003; Jones et al. 2005c). An alternative approach, recently tested in visual cortex, is likely to be most applicable for mapping interhemispheric fibers. In this method, rather than placing seed voxels in regions of high coherence (e.g., splenium of the corpus callosum), the two hemispheres were seeded separately. Only those obtained tracts that overlapped in the corpus callosum were considered to be valid tracts (Dougherty et al. 2005). This method produced anatomically plausible results for projections from primary visual cortex, but the authors cautioned that many tracts were likely missed, due to the low specificity of WMT and the resolution of current DTI acquisition protocols. New diffusion imaging methods such as DSI and QBI described above are capable of resolving regions of white matter crossing and may ultimately improve WMT in regions of complex WM.

Probabilistic Tractography Algorithms: Although deterministic streamline algorithms are nice tools for visualizing WM patterns, they provide very little information about the reliability of specific results. They rely on accurate placement of seed and deflection point ROIs by the operator, and can vary as a function of ROI size and shape, making them susceptible to generating highly errant results arising from small errors at a single step. Probabilistic tractography algorithms can overcome some of these limitations. Most probabilistic WMT algorithms are based upon some sort of iterative Monte Carlo approach where multiple trajectories are generated from the seed points with random perturbations to the trajectory directions. Model based tractography algorithms include PICo (Probability Index of Connectivity (Parker et al. 2003), which uses a fast marching technique (Parker et al. 2002), RAVE (Random Vector (Lazar and Alexander 2002)) and ProbTrack (Behrens et al. 2003b). An alternative strategy is to acquire multiple DTI datasets and use bootstrap resampling to derive data-driven estimates of probabilistic tractography (e.g., BOOT-TRAC (Lazar and Alexander 2005) (see Fig. 12). The main difference between model and data-driven approaches is that the variance of the data driven approaches will include the effects of variance in the actual data (e.g., effects of physiologic and artifact noise), not just an idealized model. All of these algorithms create a distribution of tracts, which can be used to estimate the probability of connectivity for the tractography algorithm, which may be used as a surrogate measure of WMT confidence. Additionally, connection probability may be used to segment structures such as the thalamus (Behrens et al. 2003a), cerebral peduncles (Lazar and Alexander 2005), corpus callosum

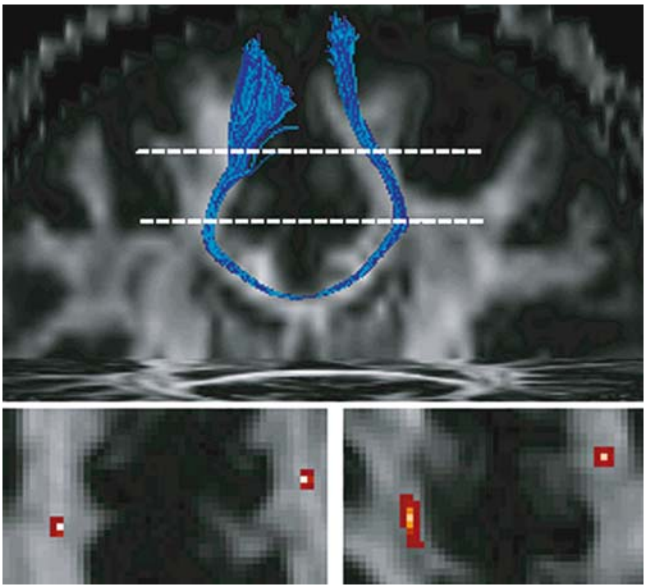

Fig. 12. Probabilistic bootstrap tractography from a single seed point in the corpus callosum illustrating the tract dispersion associated with WMT at two planes above the seed point. The estimated tract density or probability is shown using a hot color scale. The dispersion increases with distance from the seed

(Ciccarelli et al. 2003a), and cortex (Rushworth et al. 2005) according to patterns of maximum connectivity.

Diffusion Imaging and Brain Connectivity: Issues and Considerations

To date, most studies using DTI have focused on analysis of scalar tensor data (anisotropy measures, diffusivity) and have been conducted at three levels of precision: whole-brain histograms; regions-of-interest, and single-voxel analyses. Early studies focused on analysis of whole-brain histograms (e.g., Cercignani et al. 2000; Rovaris et al. 2002), which identify non-specific, global changes in diffusion properties, and may be useful for laying the foundation for more focused analyses. More recently the focus has been on region-of-interest (ROI) and voxel-based analyses. Discussion is ongoing regarding the best methods for accomplishing each type of analysis. When using ROI analyses, it is important to consider the size of the ROI being used, as large ROIs may obscure interesting changes in diffusion measures, and there is a greater possibility that the underlying anatomy will not be consistent across observations. In addition to the usual requirement that the ROIs be placed by a well-trained operator, ROI analyses of DTI data may be may be more sensitive to placement bias in the presence of disease or atrophy. This is especially the case if FA maps are used to define the ROIs. Some have attempted to minimize this potential for bias by lowering the intensity threshold on the FA maps so that local variations in FA are no longer able to guide ROI placement (e.g.,Madden et al. 2004). For voxel-based analyses, the non-diffusion weighted images ($b = 0$) are often used to register subject data to a common space (Jones et al. 2002a), but this does not guarantee that the underlying fiber architecture (defined by FA or $\hat{e}_1$) is in register. This lack of correspondence is in part due to the high inter-subject variability of the smaller fiber bundles as well as tract characteristics such as their width, neither of which are evident on the $b = 0$ images. Inter-subject variability is clear when tracts or FA maps are transformed into stereotaxic space. In Fig. 13, optic radiations

Fig. 13. Optic radiation variability ($n = 21$). Maximum overlap was 70%. Similar variability would be present if FA maps had been transformed into stereotaxic space. (Reprinted from Ciccarelli et al. 2003b, with permission from Elsevier)

were first identified using probabilistic tractography for individual subjects in native image space. The individual subject data were then resampled into a standardized space, using the b = 0 images as the reference image (Ciccarelli et al. 2003b). Similar dispersion occurs if FA maps are resampled instead of tract probabilities (Jones et al. 2002a).

The large variability across subjects away from tract centers raises the possibility that when correlations of FA and some behavioural or functional measure are found at tissue interfaces, that they may arise simply from the increased variability in FA in these regions. Many published results of voxel-based assessment of group FA differences or FA correlations have identified significant effects in regions of more variable FA. These tend to be located at interfaces of white matter with gray matter or CSF (as seen on T_1-weighted images), or in regions of complex fibre architecture. An example of one such finding is shown in Fig. 14, where correlations of FA with performance on a working-memory task were strongest at tissue interfaces. Because of the error introduced by imperfect registration, residual noise from flow artifact and partial volume effects, as well as the application of smoothing filters (see below), most authors have interpreted such findings with caution. In fact, similar concerns prompted one group to abandon a preliminary voxel-based analysis for one using tractography to define ROIs in the corpus callosum (Kanaan et al. 2006).

Results seem to be more robust to these noise sources if mean tract FA is used rather than voxel-wise FA. An example is seen in recent work examining structure-function relations in the visual system (Toosy et al. 2004). In this study, dispersion was also seen in optic radiations, and it increased as more liberal thresholds were used to define connectivity (Fig. 15, left panel). However, since the regions of high overlap (red) dominated mean FA in the optic radiations, the magnitude of the correlation of FA with the BOLD response in visual cortex was not affected (Fig. 15, right panel).

In voxel-based analyses of functional MRI data, spatial smoothing filters are typically applied to bring the statistical properties of the data more in

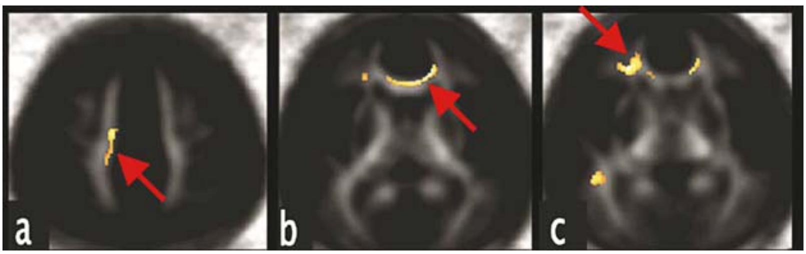

Fig. 14. Example of FA-behavior correlations at tissue interfaces. FA in fronto-parietal white matter (**a**) ranged from 0.2 to 0.6 (n = 21), and correlated with both working memory and BOLD fMRI signal intensity in superior frontal cortex. (Reprinted from Olesen et al. 2003, with permission from Elsevier)

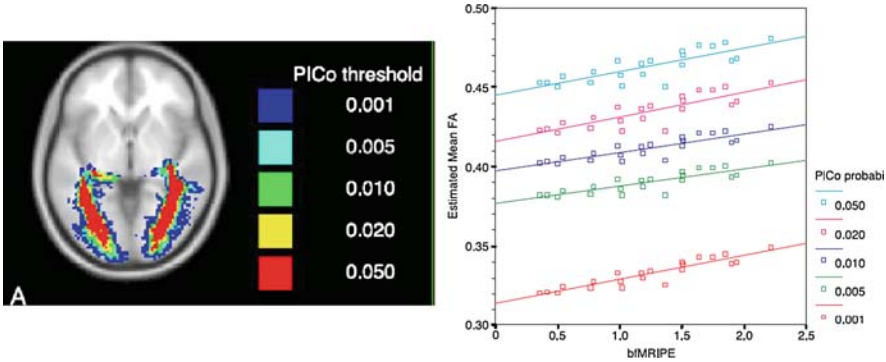

Fig. 15. Left: Optic radiation variability as a function of threshold used to define connectivity (n=22). Right: Mean FA decreased as optic radiation ROI size became larger and more dispersed, but the relation to BOLD response in visual cortex was similar. (Reprinted from Toosy et al. 2004, with permission from Elsevier)

line with random-field theory (Kiebel et al. 1999). It is not yet clear whether smoothing is appropriate for analysis of DTI data, but the size of the smoothing filter can dramatically affect residual errors and the sensitivity to detect group-wise differences (Jones et al. 2005b). In the latter study, significant FA differences between schizophrenic patients and controls were either not found, or were localized to superior temporal sulcus (STS), STS and cerebellum, or cerebellum only. This variability was due only to the size of the smoothing filter, and indicates the reasons for the choice of a specific smoothing filter should be specified.

Alternative methods for voxel-based studies have focused on registering the tensor directly (Xu et al. 2003) or tensor components (Park et al. 2003). Another approach is to use iterative registrations of FA maps to create study-specific templates (Toosy et al. 2004), as is frequently done with voxel-based-morphometry analyses (Good et al. 2001). Finally, a new method has been suggested where non-linear registration is used as the first step in aligning all subjects' FA images together; peak FA "ridges" on are found on the group-averaged FA template, creating a skeleton of the dominant WM tracts. Subject-specific FA values are then derived by finding the location in each subject's data that most closely matches the spatial location of the ridge (Smith et al. 2006, Fig. 16). This approach appears to be robust against residual misregistration since only peak FA values (corresponding to probable tract centers) are analyzed. The use of approaches that attempt to ensure better alignment of tracts across subjects or provide more robust estimates of tract-specific DTI parameters such as FA are critical to furthering our understanding of how alterations in brain connectivity affect brain function and behavior.

Tractography. Obviously, the ability of white matter tractography to estimate patterns of brain connections *in vivo* has piqued the interest of the

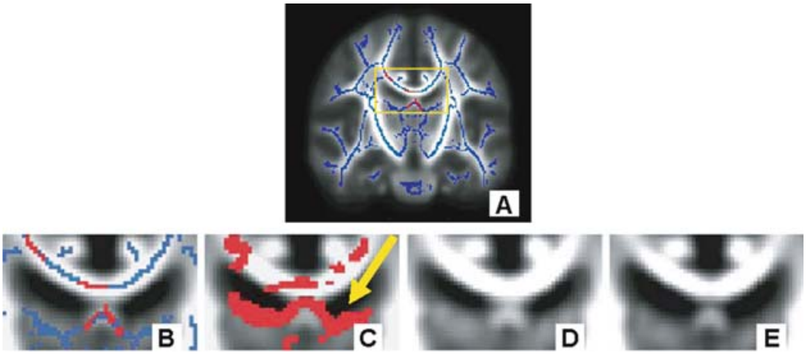

Fig. 16. (**A**) Example of an FA skeleton on a coronal FA map. The outlined region includes the cingulum bundle, corpus callosum, fornix, ventricles and thalamus and is shown in B-E. (**B**) FA skeleton is shown in blue, and significant differences between a group of controls and schizophrenics are in red. (**C**) Voxel-based analysis found additional differences at the lower edge of the ventricles (arrow). (**D**,**E**) Examination of the separate group-mean FA maps indicates this spurious finding was produced because the larger ventricles in the patient group (**E**) were not in register with the controls (**D**). Note that the corpus callosum was well-registered, and the location of FA differences more closely matched the skeletonized FA results. Images courtesy of S. Smith

neuroscience and neuroimaging communities. It is currently the only non-invasive method for reconstructing white matter trajectories in the human brain. Detailed and careful studies using white matter tractography will potentially reveal important information about brain connectivity. However, the links between tractography results, which provide information about anatomical connectivity, and measures of functional and/or effective connectivity (see below) have not yet been clearly established. Several potential anatomical measures that could influence connectivity may be derived from tractography, including the volume, length and/or cross-sectional area of the reconstructed tracts, but these are not routinely applied.

WMT has several potential applications. (1) WMT offers the unique ability to non-invasively visualize the organization of specific WM pathways in individual subjects (e.g., Fig. 11). To date, most studies of white matter neuroanatomy have been conducted using either anatomic dissection methods or axonal tracer studies in animals. The majority of tractography studies have focused on well-known and readily identifiable WM pathways such as the cortico-spinal tract, the corpus callosum and optic radiations. Many of these studies have demonstrated that WMT can generate tract reconstructions that are consistent with known neuroanatomy (e.g., Mori et al. 1999; Stieltjes et al. 2001; Catani et al. 2002; Jellison et al. 2004; Wakana et al. 2004). Recent WMT studies have moved beyond tracking prominent bundles and have attempted to determine the utility of WMT to distinguish between direct and indirect connections (Catani et al. 2003) and whether highly curved pathways near CSF can be mapped with confidence (Concha et al. 2005b). A common criticism of WMT is that the validation of these results are missing. Two approaches have been applied to address this concern – histopathological measurements and WMT have been compared in animal models (e.g., Burgel et al. 2005; Ronen et al. 2005); and measures of WMT confidence have been developed and applied to provide an estimate of the reliability of specific tractography results. It should also be noted that most neuroimaging results must be interpreted without validation. Thus it is critical to establish the reliability and repeatability of any new WMT method (e.g., Ciccarelli et al. 2003a; Ding et al. 2003; Heiervang et al. 2006). (2) WMT may be used to parcellate specific WM pathways or portions of WM pathways (see Fig. 17). This will enable tract-specific measurements such as tract volume, cross-sectional dimensions, and the statistics of quantitative measurements within the pathways such as mean diffusivity and FA. Several studies have used WMT to perform measurements in specific WM pathways: e.g., fronto-temporal connections in schizophrenia (Jones et al. 2005a; Jones et al. 2006); pyramidal tract development in newborns (Berman et al. 2005), and the pyramidal tracts and corpus callosum in multiple sclerosis (Vaithianathar et al. 2002). Concurrently, progress has been made in the development of tract-specific group templates, which may be useful for voxel-based analyses (Ciccarelli et al. 2003b; Burgel et al. 2005; Johansen-Berg et al. 2005; Thottakara et al. 2006). (3) WMT may be used to visualize specific white matter patterns relative to pathology including brain tumors, M.S. lesions, and vascular malformations. The increased

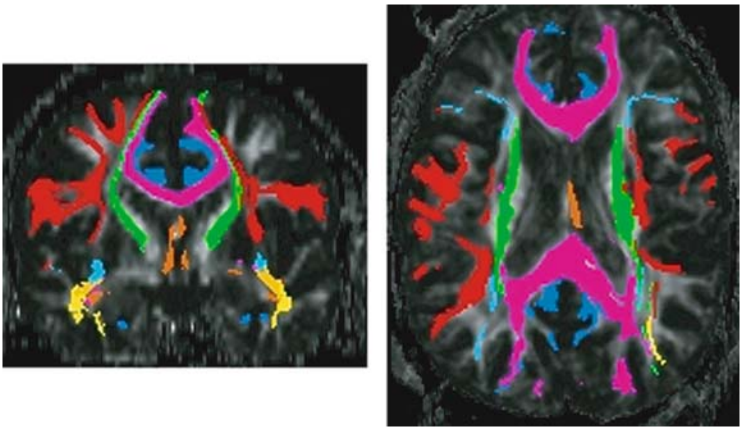

Fig. 17. Parcellation of major white matter pathways using white matter tractography in a single subject. Superior longitudinal fasciculus (*red*); corpus callosum (*purple*); inferior occipital fasciculus (*light blue*); inferior longitudinal fasciculus (*yellow*); uncinate fasciculus (*orange*); fornix/stria terminalis. (*dark orange*); corona radiata (*green*)

specificity of WM trajectories may ultimately be useful for planning surgeries (Holodny et al. 2001; Henry et al. 2004) as well as following the patterns of brain reorganization after surgery (Lazar et al. 2006). However, it should be noted that WMT reconstructions still need further validation before advocating their use as a tool for surgical guidance on a widespread basis. Indeed one recent study demonstrated that their WMT method underestimated the dimensions of the specific tract of interest (Kinoshita et al. 2005). Other studies have started to examine the relationship between specific white matter tracts affected by multiple sclerosis lesions and specific clinical impairments (Lin et al. 2005).

Integrating DTI and WMT with Function

New work is emerging that attempts to do more than simply identify differences in DTI measures as a function of some important variable such as age, disease, or performance. In these studies, the question is: what are the implications of local variations in FA and/or tract characteristics for behavior and brain activity?

Three recent studies examining correlations of local variations in FA with reaction time have found conflicting results. In an ROI analysis, FA was correlated with reaction time in a target-detection task in young and older adults. The results suggested higher FA in the splenium in younger adults and higher FA in the internal capsule in older adults were related to faster reaction times (Madden et al. 2004). Conversely, and somewhat counter intuitively, a voxel-based analysis in a different target detection task revealed primarily positive correlations: high FA was associated with longer reaction times (Tuch et al. 2005), with the strongest effects in the optic radiations. Finally, in traumatic brain injury patients, FA was not correlated with reaction time or cognitive measures, although mean diffusivity did correlate with learning and memory scores (Salmond et al. 2006). Clearly more work is required to understand these relationships.

A more integrative strategy is to examine interactions among FA, BOLD fMRI responses, and behavior or some other external variable, such as age. The few studies attempting to do this have taken a hierarchical approach (e.g., Olesen et al. 2003; Baird et al. 2005). In the first step behavior-FA and behavior-BOLD relations or BOLD activations are assessed separately, effectively reducing the analysis space by creating ROIs from significant clusters. The second step then examines BOLD-FA relations in the smaller subset of regions.

Alternatively, one could ask whether specific tracts are related to behavioural differences. Beaulieu, et al. (2005) used a voxel-based analysis to correlate FA with reading ability in a group of healthy children. The novel aspect to this work was that the authors then used the direction of the principal eigenvector in significant clusters as seeds for WMT. This allowed them to identify potential tracts passing through the significant clusters. They were able to demonstrate that the largest cluster was more likely associated with a tract not expected to be related to language processing (Fig. 18).

Finally, a number of studies have incorporated diffusion data with the results of fMRI activation studies.. The most common approach has focused on using activated clusters as starting points for tractography to identify anatomical connections. As in any tractography exercise, the choice of which activated voxels to use as seeds for tractography can result in substantially different tracts (Guye et al. 2003). The dependency of tract trajectory on the seed point chosen is compounded by the fact that significant BOLD responses are primarily measured in gray matter, which has generally has low anisotropy, and may be some number of voxels away from highly anisotropic white matter. Since regions of low anisotropy are typically excluded from fibre tracking algorithms, the user must select from nearby voxels with high FA for seeding the WMT. Because of this added uncertainty, it is even more critical to evaluate the robustness of identified tracts. Some progress in tracking between and through gray matter regions has been achieved through the use of probabilistic tractography methods that have been optimized to traverse regions of low anisotropy (e.g., Behrens and Johansen-Berg 2005).

That there is some correspondence between functional and anatomical regions has been recently shown by the Oxford group (Johansen-Berg et al. 2004). In this study, SMA (supplementary motor area) and preSMA were identified in each subject using tasks known to activate those areas independently. Probabilistic tractography was then applied to generate path probabilities from each of the two brain regions. The authors were able to show that separate groups of regions were connected to each of the BOLD regions, with little overlap, as would be expected based on known anatomy. They have recently expanded this analytical approach to show that the functional separation of

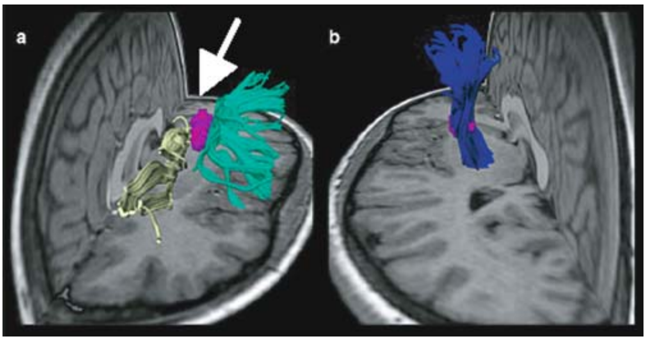

Fig. 18. (**a**) FA in the purple cluster of voxels (*arrow*) correlated with reading ability. Fibre tracking indicated this cluster was in the posterior limb of the internal capsule (**b**), and not in tracts more commonly associated with language (superior longitudinal fasiculus, in green; or superior fronto-occipital fasciculus, in yellow). (Reprinted from Beaulieu et al. 2005, with permission from Elsevier)

these two regions across subjects is more closely aligned to commonalities in local fibre architecture in adjacent white matter than to structural similarities based on conventional T_1-weighted images (Behrens et al. 2006). As the authors point out, they do not yet know if similar relations will hold in other cortical regions. Additionally, the scan time needed to acquire the high resolution DTI dataset (45 min) is not amenable for routine applications. However, the possibility for describing common patterns of functional activations based on common features in the properties of the underlying fibre architecture would be an important adjunct for understanding similarities and differences in brain connectivity.

It is important to keep in mind that DTI tractography is simply defining a model system for brain connectivity. The choice of a particular seed point will influence the derived tracts because of the inherent noise in the data acquisition and the sensitivity of the chosen algorithm to this noise. Tractography is blind to whether the seed point derives from a functional activation or from a well-placed ROI based on expert anatomical knowledge. Therefore, the tracts indicate only the possibility of an anatomical connection between a set of regions; tracts based on functional activations carry no additional "meaning" relative to those derived based on anatomical knowledge. Methods such as those being developed by the Oxford group (e.g., Behrens et al. 2006) will allow for refined anatomical models, but then the task will be to move beyond describing the possibility for information flow to describing how and when information is conveyed along the identified connections.

To fully understand brain function requires more than defining functional "blobs" correlated with some task or behavior. Methods for identifying neural systems and evaluating their interactions have been around for quite some time. Some of the earliest work examined functional connectivity using interregional correlation analyses (e.g., Clark et al. 1984; Horwitz et al. 1984); these were followed with more explicit systems-level analyses of functional and effective connectivity (e.g. Friston et al. 1993; Horwitz et al. 1999; McIntosh 2000), and more recently methods such as dynamic causal modeling (Friston et al. 2003). The importance of moving beyond identifying regions that correlate with some task or behavior has been reemphasized recently by Stephan (2004), who nicely illustrated how two brain regions can correlate independently with a task condition, but have no correlation between themselves (Fig. 19).

The possibilities for incorporating diffusion and other quantitative MRI data into analyses of functional and effective connectivity are many. However it is critical to recognize that simply demonstrating that a pathway exists between two regions that are separately related to some task or behavior does not imply nor guarantee that the identified path mediates the activity between those regions. A more fruitful strategy may be to concurrently determine the existence of pathways between *functionally* connected regions, forming the basis for models of effective connectivity. Regardless of how paths are identified, the information conveyed along those paths should be measured and assessed. Some common and readily available modeling techniques available

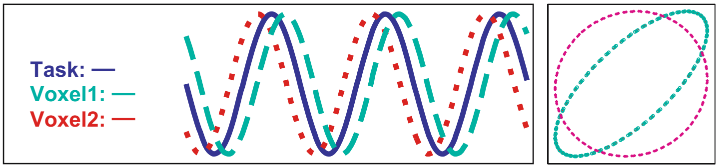

Fig. 19. A) Region A_1 (*red dotted line*) and region A_2 (*green dashed line*) are each correlated with the "task" (*blue, solid line*) at r = 0.73. B) Scatterplot showing that while the correlation of each voxel with the task is high (green, r = 0.73), the correlation between the two voxels is low (magenta, r = 0.07). Adapted from Stephan, 2004

for assessing effective connectivity are reviewed in (McIntosh 2000; Penny et al. 2004; Ramnani et al. 2004; Stephan et al. 2004; Stephan et al. 2005) See also chapters by Bressler and McIntosh, Sporns and Tononi, and Stepan and Friston in this volume. Perhaps the most important contribution from diffusion and other qMRI techniques will come from their ability to provide additional anatomical and physiological constraints to the models. Thus, the confidence that a fibre exists, its length, diameter, "integrity", and myelin content are all important contributions to the regulation of information flow between two regions. Incorporating this information into systems-level analyses of functional imaging data will greatly enhance our understanding of brain function.

Beyond Diffusion

The use of diffusion tensor imaging has become very popular in the last few years, but is not possible to know precisely from DTI studies alone the degree to which observed changes in FA reflect differential changes in myelin composition, fibre number, fibre density or other factors (e.g., Beaulieu 2002; Neil et al. 2002; Prayer and Prayer 2003). Some methods that may help distinguish among these biological properties of white matter are described in the next two sections.

2 Magnetization Transfer

Water provides the largest signal contribution to the MRI signal in brain tissues. While estimates of conductivity can be calculated from diffusion tensor data (Tuch et al. 2001), a more ideal probe of the effectiveness of white matter conduction properties would be obtained from images of myelin components. The problem is that the signals from protein and lipid molecules associated with myelin are essentially undetectable in an MRI experiment because they have ultrashort T2 values (10s of microseconds). However, the magnetization (sum of dipole moments) of free water does interact with the macromolecules through chemical exchange and dipolar coupling. This exchange of magnetic moments is referred to as magnetization transfer (Balaban and Ceckler 1992).

Magnetization transfer (MT) effects may be detected in an MRI experiment by applying strong radio-frequency (RF) pulses at a frequency shifted by roughly 1000 Hz or more from the resonance frequency of free water. The RF pulse energy will partially saturate the magnetization of the protons bound to macromolecules, which have a very broad frequency spectrum relative to that of free water (width inversely proportional to T2). The fast exchange of magnetization between the macromolecular and free water pools will indirectly attenuate the signal from the free water. The process is illustrated in Fig. 20. The attenuation is a function of the amplitude, rate, and frequency offset of the RF attenuation pulses, and the concentration of macromolecules and exchange rate of the magnetization between the free water and bound macromolecular pools.

The most common approach for characterizing MT is to acquire two sets of images – one with the off-resonance saturation MT pulses (Ms) and one set without (Mo). The MT contrast (MTC) is the difference between the images, MTC = Mo − Ms. Since absolute signal intensities are arbitrary, the MTC is typically normalized by the signal without MT saturation, which is the MT ratio

$$\mathrm{MTR} = (\mathrm{Mo} - \mathrm{Ms})/\mathrm{Mo} \tag{16}$$

The MTR is the most commonly used measure of magnetization transfer and example maps are shown in Fig. 21. Increased MTR values may correspond to increased macromolecular concentrations in the tissue. The MTR values in healthy WM and GM are roughly 0.4-0.55 and 0.25–0.35, respectively. The higher MTR in WM is believed to be associated with the proteins and lipids associated with myelinated axons (Stanisz et al. 1999). Consequently, the MTR in WM is reduced in demyelinating diseases such as multiple sclerosis

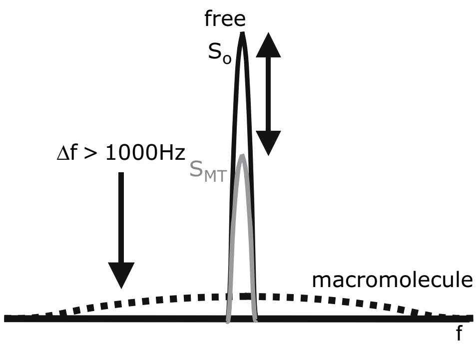

Fig. 20. Schematic of the MT saturation process. An intense RF pulse is applied off-resonance, which saturates the magnetization of the macromolecule pool. Rapid exchange between magnetization of the macromolecule pool and the free water pool causes the free water signal to be partially attenuated

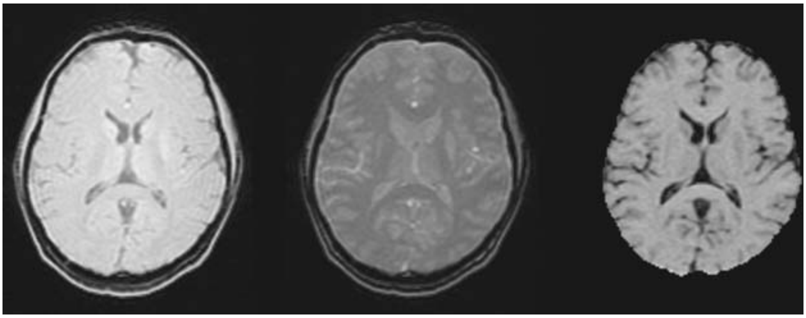

Fig. 21. Example images from an MTR experiment. The image on the left was obtained without any MT saturation. The MT-weighted image in the middle was obtained by applying a 90° pulse 3000 Hz off-resonance (TR = 30 ms). The image on the right is the estimated MT ratio (MTR) map using Equation 16. Images courtesy of A. Samsonov and A. Field

although the MTR can also be influenced by overall water content and other macromolecules in processes such as neuroinflammation (Stanisz et al. 2004).

MT saturation is achieved using an RF pre-pulse, which may be applied in combination with any RF pulse sequence o. An example spin-echo CPMG pulse sequence with RF saturation is shown in Fig. 22. There has been considerable variation of reported MTR properties in the literature, which is likely caused by inconsistencies in the pulse sequence protocols. The exact MTR measurement will depend upon the pulse sequence parameters (e.g., TR, TE, excitation flip angle), the magnetic field strength, as well as the shape, amplitude and frequency offset of the saturation pulses. Consequently, within a single MTR study, the imaging parameters should be fixed to maximize consistency. Common problems with MTR experiments include spatial inhomogeneities in both the static magnetic field (B0) and the RF magnetic field (B1).

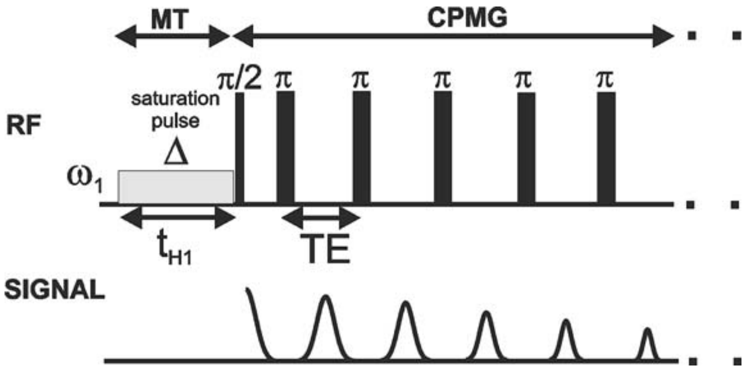

Fig. 22. Measurement of T_2 relaxation in the presence and absence of an RF saturation pulse. Courtesy of G.J. Stanisz

B0 inhomogeneities are caused by poor shimming and spatial variations in the magnetic susceptibilities in soft tissue, bone and air, which lead to shifts (errors) in the saturation frequency offsets. Inhomogeneities in the B1 field, which are common using volume head coils particularly at high magnetic fields (B0 > 1.5T) will affect the saturation pulse amplitude and consequently alter the level of MT saturation. Both B0 and B1 fields may be measured and used to retrospectively correct MTR measurements (Sled and Pike 2000; Ropele et al. 2005) Another source of MT saturation is the application of RF excitation pulses for slice selection in 2D pulse sequences (Santyr 1993). The slice selective RF pulses of other slices shifted relative to the current one will cause MT saturation. This is more problematic for multi-slice 2D pulse sequences with many 180° pulses (e.g., fast spin echo, and T1-weighted spin echo); therefore, 3D scans are generally preferable for MTR measurements. Other considerations for MTR measurements are discussed in two excellent review papers (Henkelman et al. 2001; Horsfield et al. 2003).

As discussed above, the MTR measurement is highly dependent upon a broad range of pulse sequence and scanner factors. Consequently, several research groups have been developing models and imaging protocols for quantitative measurements of MT properties (Henkelman et al. 1993; Stanisz et al. 1999; Sled and Pike 2001; Yarnykh 2002; Tozer et al. 2003; Yarnykh and Yuan 2004). these techniques typically require measurements at multiple frequency offsets and saturation pulse amplitudes. Since MT saturation is performed using RF pulses, the MT models are usually based upon a two-pool model (free water and macromolecule) with continuous RF saturation approximated by regular RF saturation pulses. By using these models, it is possible to estimate the macromolecular concentration (bound pool fraction), the exchange rate between the free and bound pools, and the T2 of the bound pool (Fig. 23). Unfortunately, the acquisition of the required images can be quite time consuming, which has limited the overall applicability of the technique. Nonetheless, quantitative MT methods are much more specific than the conventional MTR methods.

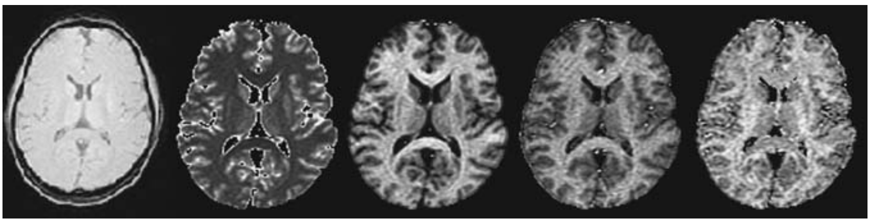

Fig. 23. Quantitative MT maps obtained by acquiring data at multiple frequency offsets and flip angles and using a two pool (free water and macromolecule) model with exchange. The images from left to right are: no MT contrast, T1 map, exchange rate (k), bound pool fraction (f_b), and the T2 of the bound pool ($T2_b$). The images demonstrate the wide range of quantitative imaging measures that can be obtained in a quantitative MT experiment. Images courtesy of A. Samsonov and A. Field

Relationship to Behavioural and Neural Functioning

As for FA, MTR is a non-specific marker of neural damage, such as demyelination. Many of the published MT studies have focused on patients with multiple sclerosis, who show decreased MT in both ROI and whole-brain histogram analyses. In other diseases, results are similar, indicating MTR is a viable marker for affected white and gray matter. MTR has been shown to increase with brain development during the first several years of life (Rademacher et al. 1999; van Buchem et al. 2001) and regional decreases with aging have been found (Armstrong et al. 2004). Differences in MTR were sufficiently large to distinguish patients with mild cognitive impairment from patients with Alzheimer's disease and controls (Kabani et al. 2002a; Kabani et al. 2002b). A number of published studies have also used magnetization transfer methods to compare the brains in patients with schizophrenia against healthy control subjects (Foong et al. 2001; Bagary et al. 2003; Kiefer et al. 2004; Kubicki et al. 2005). Reduced MTR measurements have also been observed in a small sample of patients with late-life major depressive disorders (Kumar et al. 2004).

Only a few studies have attempted to relate magnetization transfer measurements to measures reflecting brain function. A serial MTR study in the optic nerves of 29 patients with acute optic neuritis was performed with measurements of visual system functioning using visual evoked potentials (VEP) (Hickman et al. 2004). No significant differences in MTR were observed between patients and controls at the onset of optic neuritis, although the MTR did decrease in patients over a period of one year. There did not seem to be any direct relationship between MTR and VEP measurements. Another study of 18 patients with early-stage multiple sclerosis (Au Duong et al. 2005) demonstrated a correlation between functional connectivity between left Brodmann areas 45/46 and 24 using an fMRI working memory task, and the MTR of normal appearing white matter and also with brain T2 lesion load. Consequently, the functional connectivity relationship with MTR suggests that changes in the functional working memory network is related to changes in the white matter pathophysiology. A combined MTR and fMRI study (Filippi et al. 2002) of simple motor function in patients with multiple sclerosis revealed correlations between the MTR histogram features of whole-brain, normal appearing brain tissue (both GM and WM) and fMRI signal strengths in ipsilateral sensorimotor cortex and supplementary motor area (bilaterally). The fMRI signal in contralateral sensorimotor cortex was significantly correlated with MTR histogram features in patients with cervical but not dorsal spinal cord myelitis (Rocca et al. 2005). Finally, a recent study measured diffusion and MT in patients with schizophrenia (Kalus et al. 2005). The amygdala showed lower anisotropy (inter-voxel coherence), and differences in quantitative MT measures (T_1, fraction bound pool), but not MTR. The authors interpreted the findings as indicating a possible increase in neuronal density in the amygdala of schizophrenics. The functional significance of these changes is not clear, however, as there were no significant correlations of any of the quantitative MR measures with disease duration or symptom severity.

3 T1 and T2 Relaxometry

Contrast in most human neuroimaging studies is a function of the T1 and T2 relaxation times of the brain tissues. Consequently, regional signal differences in brain images are often caused by differences in the relaxation properties. T1 is the recovery time of the longitudinal magnetization and T2 is the decay constant associated with the transverse magnetization. Both characteristic times are highly sensitive to bulk water of the tissue and tend to increase with water content. Significant changes in both T1 and T2 are observed with early brain maturation (e.g., Miot et al. 1995; Miot-Noirault et al. 1997; Sie et al. 1997; Steen et al. 1997; Paus et al. 2001) and aging (Jernigan et al. 1991; Autti et al. 1994; Salonen et al. 1997). In development, these changes are likely caused by decreased water content and increased water binding and compartmentalization including during premyelination periods when lipids, proteins, and glial cells are increasing. T2 appears to be more sensitive to the changes associated with brain maturation although T1 changes have been reported to be more closely linked to the onset of myelination (e.g., Barkovich et al. 1988; Martin et al. 1988).

There are two principle approaches for measuring T1– inversion recovery and variable saturation. The inversion recovery methods work by inverting the longitudinal magnetization with a 180° pulse and then obtaining measurements with different inversion times. Variable saturation methods work by obtaining measurements with either several RF excitation flip angles or several different TR periods. All methods are highly sensitive to the accuracy of the RF magnetic field, although new analytical methods can retrospectively correct for inhomogeneities (Cheng and Wright 2006).

T2 is generally measured using spin echo pulse sequences, where measurements are obtained at different TE (echo times). The signal decay is governed by the equation S = So exp(-TE/T2). The most efficient method is to use a multiple spin-echo pulse sequence, where measurements are obtained at multiple TE values for a single excitation, although there continue to be lively discussions in the literature concerning the appropriate number and spacing of echos for quantitative T_2 calculations (e.g., Duncan et al. 1996; Whittall et al. 1999; Townsend et al. 2004), related primarily to the nature of T_2 decay (see below). The measurement of T_2 is also highly sensitive to imperfections in the RF and static magnetic fields (Poon and Henkelman 1995). Further, the RF imperfections will also lead to stimulated echoes in multi-echo sequences, which are governed by T1, which can lead to overestimation of the T2. The stimulated echo components can be suppressed using variable amplitude gradient crusher pulses around each 180° refocusing pulse (Poon and Henkelman 1995). As for MT, the accuracy of T2 measurements will depend on these parameters, so if the number of echos possible are limited, they should be chosen with care (Duncan et al. 1996).

In spite of the fact that T1 and T2 are highly sensitive to a wide range of tissue factors, and are therefore likely to be nonspecific, relaxation time measurements have been shown to be affected in many neurological diseases that have impairments in connectivity including epilepsy, substance abuse and neurodegenerative diseases such as M.S., dementia, schizophrenia, Alzheimer's disease, Parkinson's disease. One potentially confounding factor in many of these studies is the presence of edema, which will increase the bulk water content in the tissue. To date, only one study has specifically related relaxation time measurements to measures of brain connectivity (Vaithianathar et al. 2002). In this study of MS patients, DTI was used to identify the pyramidal tracts and fibers passing through the corpus callosum. Histograms of T_1 relaxation data along the pathways were generated and indicated decreased T_1 relaxivity in patients relative to controls. There was no correlation of T_1 relaxation in these paths with standard clinical disability rating scale scores, and no cognitive measures were available for analysis.

Myelin Water Fraction

Although the specificity of T1 and T2 measurements are generally perceived as being poor, several investigators have recently shown that the T2 signal decay in neural tissue is multi-exponential with echo time (Menon and Allen 1991; MacKay et al. 1994; Whittall et al. 1997). Further investigation has shown that different water tissue compartments each have distinct T2 characteristics, and may be separated (see Fig. 24). In white matter, the water signal compartments are believed to originate from components of free water (e.g., edema, CSF, which have long T2 $>$ 120 ms), extracellular water (T2 $\sim$ 60–90 ms) and water within the myelin membranes of axons (T2 $\sim$ 10–40 ms) (MacKay et al. 1994; Beaulieu et al. 1998; Stanisz and Henkelman 1998; Vavasour et al. 1998; Laule et al. 2004). The T_2 of the extracellular fraction can be used to identify inflamed neural tissues (Stanisz et al. 2004), and the latter component is of significant interest because it is specific to myelin, which is critical for signal conduction in the brain. Consequentially, a potentially important biomarker is the myelin water fraction, which is the total signal

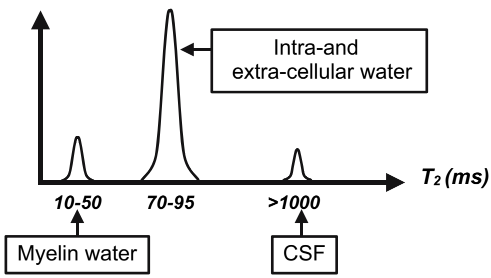

Fig. 24. T2 spectrum of water signal in white matter. The water in the myelin layers has a very short T2 (between 10 and 50 ms), intra- and extra-cellular water have intermediate T2 values, and CSF and unrestricted water pools have much longer T2 values

from the short T2 signal component relative to the total signal from both the short and intermediate tissue signal components. In healthy adult WM, the myelin water fraction (MWF) is typically 6–15% dependent upon the region (Whittall et al. 1997). A representative map of MWF is shown in Fig. 25.

Measurements of MWF are usually obtained using a 2D multiple spin echo sequence, which consists of a train of equally spaced 180° refocusing pulses (Poon and Henkelman 1992; Poon and Henkelman 1995; Whittall et al. 1997). T2 measurements are highly sensitive to errors in the RF magnetic field, which are problematic for typical slice-selective RF refocusing pulses. Consequently, non-selective refocusing pulses are often used, which limits the acquisition to a single 2D slice. Variable amplitude crusher gradient pulses are typically placed around each refocusing pulse to suppress the signal from stimulated echoes. The fitting of the T2 model is also highly sensitive to image noise; consequently, long scan times are typically required to achieve sufficient SNR. Different strategies exist for fitting the T2 signal decay to a multi-exponential function (e.g., Stanisz and Henkelman 1998; Webb et al. 2003; Jones et al. 2004) although the non-negative least squares (NNLS) method is probably most commonly used (Whittall et al. 1997). The slow acquisition time (typically > 10 minutes) for a single 2D slice has ultimately limited the application of this approach. However, one consideration is that the 2D imaging times are in line with MR spectroscopy. Further, the MWF is one of the more specific measures of white matter tissue properties, which makes it promising for correlations with measures of brain connectivity. Careful selection of echos in conventional pulse sequences may provide reasonable myelin maps (Vidarsson et al. 2005; Oh et al. 2006), although the option to acquire such data is not available routinely on most clinical scanners. Future

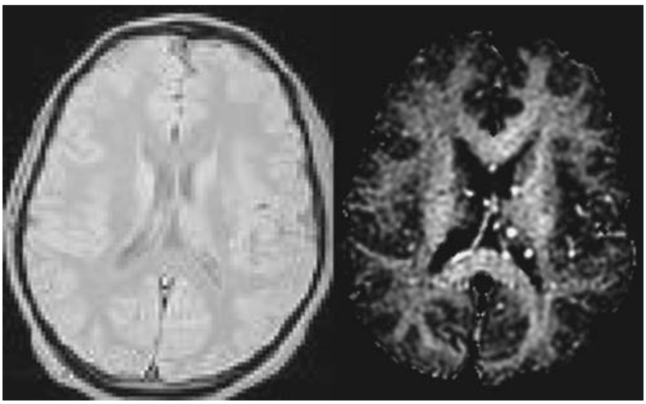

Fig. 25. Maps from a myelin water fraction experiment. The image on the left is a proton-density weighted image obtained from the first TE (8 ms) in the CPMG echo train. The map on the right is the estimated myelin water fraction image at the same slice location. Note that the myelin water fraction is much higher in regions of white matter

developments are clearly needed to improve both the acquisition speed and spatial coverage of the technique, which are somewhat at odds with one another. Imaging at higher magnetic field strengths, with better RF coils, parallel imaging and 3D pulse sequences may ultimately improve the utility of the method.

To date, no studies have been performed which have related MWF measurements to measures of brain connectivity. However, MWF measurements in WM have been shown to be affected in brain diseases with aberrant brain connectivity behavior including schizophrenia (Flynn et al. 2003) and multiple sclerosis (Vavasour et al. 1998; Gareau et al. 2000; Whittall et al. 2002; Laule et al. 2004; Tozer et al. 2005).

4 Discussion and Future Directions

In this chapter, we have described several quantitative MRI measures, which are promising for the characterization of brain connectivity. However, to date, there has been a relative paucity of experiments that have directly compared functional and effective measures of brain connectivity with these structural and anatomical measures of brain connectivity and physiology. This is likely to change in the near future as these techniques become more available. Characterization of WM anatomy and physiology with MRI may enable more complex models of brain connectivity to be developed, as the circuitry of brain connectivity becomes more well-defined. For example, many have proposed that FA increases are primarily reflecting myelination. This leads to the prediction that FA would be correlated most strongly with the short myelin-water fraction from T_2 relaxometry experiments, as well as to the size of the macromolecular pool in quantitative MT studies. On the other hand, if changes in fibre density underlie changes in FA (Beaulieu 2002), FA should be more strongly associated with the extracellular water peak. Preliminary evidence for this prediction comes from recent work showing FA was not correlated with the myelin water fraction in white matter (MacKay et al. 2006). Functional and effective connectivity studies so far have generally modeled the brain as a "black box" with inputs and outputs, and most of the internal circuitry has been derived from non-human primate studies. Quantitative structural and physiological image data from MRI may provide critical information about the functional circuitry within the black box.

To move quantitative MRI into the forefront of techniques for characterizing brain connectivity, further developments are necessary. Obviously, improvements to both the imaging technology through better and more efficient pulse sequences, imaging RF coils, and gradient coils, and quantitative imaging models and image analysis methods will facilitate comparisons between more conventional connectivity measures with quantitative MRI measures of WM. However, even with improvements in the technology, the application will be somewhat limited unless they become more readily available, either through the MRI system manufacturers or through research collaborations. While the methodologies are still young and emerging, we can already pose some interesting questions: Do variations in diffusion parameters or myelin content along tracts relate to function? Is the whole fibre tract affected? Does knowing something about tract likelihood help predict differences in functional and effective connectivity? Answers to these and similar questions will require multimodal imaging, as most quantitative MRI studies have focused on a single measure or measurement type We will also need a better understanding of the statistical properties of the data, and sophisticated multivariate and nonlinear modeling techniques, some of which are already available, and others of which are discussed throughout this volume. This will be an iterative process and will require refinement of both imaging and analysis techniques. However, we have optimism that in the end the model fits will be acceptable and we will know something useful about how brain structure contributes to brain function.

Acknowledgements

The authors would like to thank Mariana Lazar, Yu-Chien Wu, Alexey Samsonov, Yijing Wu, and Aaron Field at the University of Wisconsin for providing figures, as well as Steve Smith from Oxford and Greg Stanisz from Sunnybrook Health Sciences Centre, and thanks also to Ana Solodkin at the University of Chicago for lively discussions. Some of the diffusion MRI work presented here was supported by NIH grant RO1 MH 62015 and the MT and MWF data was generated from a grant from the National Multiple Sclerosis Society (University of Wisconsin).

References

Abe O, Aoki S, Hayashi N, Yamada H, Kunimatsu A, Mori H, Yoshikawa T, Okubo T, Ohtomo K (2002) Normal aging in the central nervous system: quantitative MR diffusion-tensor analysis. Neurobiology of Aging 23: 433–441

Adler CM, Holland SK, Schmithorst V, Wilke M, Weiss KL, Pan H, Strakowski SM (2004) Abnormal frontal white matter tracts in bipolar disorder: a diffusion tensor imaging study. Bipolar Disorders 6: 197–203

Agartz I, Andersson JL, Skare S (2001) Abnormal brain white matter in schizophrenia: a diffusion tensor imaging study. Neuroreport 12: 2251–2254

Alexander AL, Hasan K, Kindlmann G, Parker DL, Tsuruda JS (2000) A geometric analysis of diffusion tensor measurements of the human brain. Magnetic Resonance in Medicine 44: 283–291

Alexander AL, Hasan KM, Lazar M, Tsuruda JS, Parker DL (2001a) Analysis of partial volume effects in diffusion-tensor MRI. Magnetic Resonance in Medicine 45: 770–780

Alexander AL, Tsuruda JS, Parker DL (1997) Elimination of eddy current artifacts in diffusion-weighted echo-planar images: the use of bipolar gradients. Magnetic Resonance in Medicine 38: 1016–1021

Alexander DC, Barker GJ, Arridge SR (2002) Detection and modeling of non-Gaussian apparent diffusion coefficient profiles in human brain data. Magnetic Resonance in Medicine 48: 331–340

Alexander DC, Pierpaoli C, Basser PJ, Gee JC (2001b) Spatial transformations of diffusion tensor magnetic resonance images. IEEE Transactions on Medical Imaging 20: 1131–1139

Anderson AW (2001) Theoretical analysis of the effects of noise on diffusion tensor imaging. Magnetic Resonance in Medicine 46: 1174–1188

Andersson JL, Skare S (2002) A model-based method for retrospective correction of geometric distortions in diffusion-weighted EPI. Neuroimage 16: 177–199

Armstrong CL, Traipe E, Hunter JV, Haselgrove JC, Ledakis GE, Tallent EM, Shera D, van Buchem MA (2004) Age-related, regional, hemispheric, and medial-lateral differences in myelin integrity in vivo in the normal adult brain. AJNR: American Journal of Neuroradiology 25: 977–984

Assaf Y, Ben-Bashat D, Chapman J, Peled S, Biton IE, Kafri M, Segev Y, Hendler T, Korczyn AD, Graif M, Cohen Y (2002a) High b-value q-space analyzed diffusion-weighted MRI: application to multiple sclerosis. Magnetic Resonance in Medicine 47: 115–126

Assaf Y, Chapman J, Ben-Bashat D, Hendler T, Segev Y, Korczyn AD, Graif M, Cohen Y (2005) White matter changes in multiple sclerosis: correlation of q-space diffusion MRI and 1H MRS. Magnetic Resonance Imaging 23: 703–710

Assaf Y, Freidlin RZ, Rohde GK, Basser PJ (2004) New modeling and experimental framework to characterize hindered and restricted water diffusion in brain white matter. Magnetic Resonance in Medicine 52: 965–978

Assaf Y, Kafri M, Shinar H, Chapman J, Korczyn AD, Navon G, Cohen Y (2002b) Changes in axonal morphology in experimental autoimmune neuritis as studied by high b-value q-space (1)H and (2)H DQF diffusion magnetic resonance spectroscopy. Magnetic Resonance in Medicine 48: 71–81

Assaf Y, Mayzel-Oreg O, Gigi A, Ben-Bashat D, Mordohovitch M, Verchovsky R, Reider G, II, Hendler T, Graif M, Cohen Y, Korczyn AD (2002c) High b value q-space-analyzed diffusion MRI in vascular dementia: a preliminary study. Journal of the Neurological Sciences 203–204: 235–239

Au Duong MV, Audoin B, Boulanouar K, Ibarrola D, Malikova I, Confort-Gouny S, Celsis P, Pelletier J, Cozzone PJ, Ranjeva JP (2005) Altered functional connectivity related to white matter changes inside the working memory network at the very early stage of MS. Journal of Cerebral Blood Flow and Metabolism 25: 1245–1253

Autti T, Raininko R, Vanhanen SL, Kallio M, Santavuori P (1994) MRI of the normal brain from early childhood to middle age. II. Age dependence of signal intensity changes on T2-weighted images. Neuroradiology 36: 649–651

Bagary MS, Symms MR, Barker GJ, Mutsatsa SH, Joyce EM, Ron MA (2003) Gray and white matter brain abnormalities in first-episode schizophrenia inferred from magnetization transfer imaging. Archives of General Psychiatry 60: 779–788

Baird AA, Colvin MK, Vanhorn JD, Inati S, Gazzaniga MS (2005) Functional connectivity: integrating behavioral, diffusion tensor imaging, and functional magnetic resonance imaging data sets. Journal of Cognitive Neuroscience 17: 687–693

Balaban RS, Ceckler TL (1992) Magnetization transfer contrast in magnetic resonance imaging. Magnetic Resonance Quarterly 8: 116–137

Barkovich AJ, Kjos BO, Jackson DE, Jr., Norman D (1988) Normal maturation of the neonatal and infant brain: MR imaging at 1.5 T. Radiology 166: 173–180

Barnea-Goraly N, Eliez S, Hedeus M, Menon V, White CD, Moseley M, Reiss AL (2003) White matter tract alterations in fragile X syndrome: preliminary evidence from diffusion tensor imaging. American Journal of Medical Genetics Part B: Neuropsychiatric Genetics 118: 81–88

Barnea-Goraly N, Kwon H, Menon V, Eliez S, Lotspeich L, Reiss AL (2004) White matter structure in autism: preliminary evidence from diffusion tensor imaging. Biological Psychiatry 55: 323–326

Barnea-Goraly N, Menon V, Eckert M, Tamm L, Bammer R, Karchemskiy A, Dant CC, Reiss AL (2005) White matter development during childhood and adolescence: A cross-sectional diffusion tensor imaging study. Cerebral Cortex 15: 1848–1854

Basser PJ, Mattiello J, LeBihan D (1994) Estimation of the effective self-diffusion tensor from the NMR spin echo. Journal of Magnetic Resonance Series B 103: 247–254

Basser PJ, Pajevic S, Pierpaoli C, Duda J, Aldroubi A (2000) In vivo fiber tractography using DT-MRI data. Magnetic Resonance in Medicine 44: 625–632

Basser PJ, Pierpaoli C (1996) Microstructural and physiological features of tissues elucidated by quantitative-diffusion-tensor MRI. Journal of Magnetic Resonance Series B 111: 209–219

Basser PJ, Pierpaoli C (1998) A simplified method to measure the diffusion tensor from seven MR images. Magnetic Resonance in Medicine 39: 928–934

Bastin ME (2001) On the use of the FLAIR technique to improve the correction of eddy current induced artefacts in MR diffusion tensor imaging. Magnetic Resonance Imaging 19: 937–950

Batchelor PG, Atkinson D, Hill DL, Calamante F, Connelly A (2003) Anisotropic noise propagation in diffusion tensor MRI sampling schemes. Magnetic Resonance in Medicine 49: 1143–1151

Beaulieu C (2002) The basis of anisotropic water diffusion in the nervous system - a technical review. NMR in Biomedicine 15: 435–455

Beaulieu C, Fenrich FR, Allen PS (1998) Multicomponent water proton transverse relaxation and T2-discriminated water diffusion in myelinated and nonmyelinated nerve. Magnetic Resonance Imaging 16: 1201–1210

Beaulieu C, Plewes C, Paulson LA, Roy D, Snook L, Concha L, Phillips L (2005) Imaging brain connectivity in children with diverse reading ability. Neuroimage 25: 1266–1271

Behrens TE, Jenkinson M, Robson MD, Smith SM, Johansen-Berg H (2006) A consistent relationship between local white matter architecture and functional specialisation in medial frontal cortex. Neuroimage 30: 220–227

Behrens TE, Johansen-Berg H (2005) Relating connectional architecture to grey matter function using diffusion imaging. Philosophical transactions of the Royal Society of London. Series B, Biological sciences 360: 903–911

Behrens TE, Johansen-Berg H, Woolrich MW, Smith SM, Wheeler-Kingshott CA, Boulby PA, Barker GJ, Sillery EL, Sheehan K, Ciccarelli O, Thompson AJ, Brady JM, Matthews PM (2003a) Non-invasive mapping of connections between human thalamus and cortex using diffusion imaging. Nature Neuroscience 6: 750–757

Behrens TE, Woolrich MW, Jenkinson M, Johansen-Berg H, Nunes RG, Clare S, Matthews PM, Brady JM, Smith SM (2003b) Characterization and propagation of uncertainty in diffusion-weighted MR imaging. Magnetic Resonance in Medicine 50: 1077–1088

Berman JI, Mukherjee P, Partridge SC, Miller SP, Ferriero DM, Barkovich AJ, Vigneron DB, Henry RG (2005) Quantitative diffusion tensor MRI fiber tractography of sensorimotor white matter development in premature infants. Neuroimage 27: 862–871

Beyer JL, Taylor WD, MacFall JR, Kuchibhatla M, Payne ME, Provenzale JM, Cassidy F, Krishnan KR (2005) Cortical white matter microstructural abnormalities in bipolar disorder. Neuropsychopharmacology 30: 2225–2229

Brugieres P, Thomas P, Maraval A, Hosseini H, Combes C, Chafiq A, Ruel L, Breil S, Peschanski M, Gaston A (2004) Water diffusion compartmentation at high b values in ischemic human brain. AJNR: American Journal of Neuroradiology 25: 692–698

Buchsbaum MS, Tang CY, Peled S, Gudbjartsson H, Lu D, Hazlett EA, Downhill J, Haznedar M, Fallon JH, Atlas SW (1998) MRI white matter diffusion anisotropy and PET metabolic rate in schizophrenia. Neuroreport 9: 425–430

Burgel U, Amunts K, Hoemke L, Mohlberg H, Gilsbach JM, Zilles K (2005) White matter fiber tracts of the human brain: Three-dimensional mapping at microscopic resolution, topography and intersubject variability. Neuroimage

Callaghan PT (1994) Principles of Magnetic Resonance Microscopy Oxford University Press, Oxford

Catani M, Howard RJ, Pajevic S, Jones DK (2002) Virtual in vivo interactive dissection of white matter fasciculi in the human brain. Neuroimage 17: 77–94

Catani M, Jones DK, Donato R, Ffytche DH (2003) Occipito-temporal connections in the human brain. Brain 126: 2093–2107

Cercignani M, Iannucci G, Rocca MA, Comi G, Horsfield MA, Filippi M (2000) Pathologic damage in MS assessed by diffusion-weighted and magnetization transfer MRI. Neurology 54: 1139–1144

Chang LC, Jones DK, Pierpaoli C (2005) RESTORE: robust estimation of tensors by outlier rejection. Magnetic Resonance in Medicine 53: 1088–1095

Chenevert TL, Brunberg JA, Pipe JG (1990) Anisotropic diffusion in human white matter: demonstration with MR techniques in vivo. Radiology 177: 401–405

Cheng HL, Wright GA (2006) Rapid high-resolution T(1) mapping by variable flip angles: accurate and precise measurements in the presence of radiofrequency field inhomogeneity. Magnetic Resonance in Medicine 55: 566–574

Ciccarelli O, Parker GJ, Toosy AT, Wheeler-Kingshott CA, Barker GJ, Boulby PA, Miller DH, Thompson AJ (2003a) From diffusion tractography to quantitative white matter tract measures: a reproducibility study. Neuroimage 18: 348–359

Ciccarelli O, Toosy AT, Parker GJ, Wheeler-Kingshott CA, Barker GJ, Miller DH, Thompson AJ (2003b) Diffusion tractography based group mapping of major white-matter pathways in the human brain. Neuroimage 19: 1545–1555

Clark CM, Kessler R, Buchsbaum MS, Margolin RA, Holcomb HH (1984) Correlational methods for determining regional coupling of cerebral glucose metabolism. A pilot study. Biological Psychiatry 19: 663–678

Cohen Y, Assaf Y (2002) High b-value q-space analyzed diffusion-weighted MRS and MRI in neuronal tissues - a technical review. NMR in Biomedicine 15: 516–542

Concha L, Beaulieu C, Gross DW (2005a) Bilateral limbic diffusion abnormalities in unilateral temporal lobe epilepsy. Annals of Neurology 57: 188–196

Concha L, Gross DW, Beaulieu C (2005b) Diffusion tensor tractography of the limbic system. AJNR: American Journal of Neuroradiology 26: 2267–2274

Conturo TE, Lori NF, Cull TS, Akbudak E, Snyder AZ, Shimony JS, McKinstry RC, Burton H, Raichle ME (1999) Tracking neuronal fiber pathways in the living human brain. Proceedings of the National Academy of Sciences of the United States of America 96: 10422–10427

Conturo TE, McKinstry RC, Akbudak E, Robinson BH (1996) Encoding of anisotropic diffusion with tetrahedral gradients: a general mathematical diffusion formalism and experimental results. Magnetic Resonance in Medicine 35: 399–412

Ding Z, Gore JC, Anderson AW (2003) Classification and quantification of neuronal fiber pathways using diffusion tensor MRI. Magnetic Resonance in Medicine 49: 716–721

Dougherty RF, Ben-Shachar M, Bammer R, Brewer AA, Wandell BA (2005) Functional organization of human occipital-callosal fiber tracts. Proceedings of the National Academy of Sciences of the United States of America 102: 7350–7355

Duncan JS, Bartlett P, Barker GJ (1996) Technique for measuring hippocampal T2 relaxation time. AJNR: American Journal of Neuroradiology 17:1805–1810

Einstein A (1926) Investigations on the Theory of the Brownian Movement. Methuen and Co.

Ellis CM, Simmons A, Jones DK, Bland J, Dawson JM, Horsfield MA, Williams SC, Leigh PN (1999) Diffusion tensor MRI assesses corticospinal tract damage in ALS. Neurology 53: 1051–1058

Field AS, Alexander AL, Wu YC, Hasan KM, Witwer B, Badie B (2004) Diffusion tensor eigenvector directional color imaging patterns in the evaluation of cerebral white matter tracts altered by tumor. Journal of Magnetic Resonance Imaging 20: 555–562

Filippi M, Rocca MA, Falini A, Caputo D, Ghezzi A, Colombo B, Scotti G, Comi G (2002) Correlations between structural CNS damage and functional MRI changes in primary progressive MS. Neuroimage 15: 537–546

Flynn SW, Lang DJ, Mackay AL, Goghari V, Vavasour IM, Whittall KP, Smith GN, Arango V, Mann JJ, Dwork AJ, Falkai P, Honer WG (2003) Abnormalities of myelination in schizophrenia detected in vivo with MRI, and post-mortem with analysis of oligodendrocyte proteins. Molecular Psychiatry 8: 811–820

Foong J, Symms MR, Barker GJ, Maier M, Woermann FG, Miller DH, Ron MA (2001) Neuropathological abnormalities in schizophrenia: evidence from magnetization transfer imaging. Brain 124 (Pt 5): 882–892

Frank LR (2002) Characterization of anisotropy in high angular resolution diffusion-weighted MRI. Magnetic Resonance in Medicine 47: 1083–1099

Friston KJ, Frith CD, Liddle PF, Frackowiak RSJ (1993) Functional connectivity: the principal-component analysis of large (PET) data sets. Journal of Cerebral Blood Flow and Metabolism 13: 5–14

Friston KJ, Harrison L, Penny W (2003) Dynamic causal modelling. Neuroimage 19: 1273–1302

Gareau PJ, Rutt BK, Karlik SJ, Mitchell JR (2000) Magnetization transfer and multicomponent T2 relaxation measurements with histopathologic correlation in an experimental model of MS. Journal of Magnetic Resonance Imaging 11: 586–595

Good CD, Johnsrude IS, Ashburner J, Henson RN, Friston KJ, Frackowiak RS (2001) A voxel-based morphometric study of ageing in 465 normal adult human brains. Neuroimage 14: 21–36

Gudbjartsson H, Maier SE, Jolesz FA (1997) Double line scan diffusion imaging. Magnetic Resonance in Medicine 38: 101–109

Guye M, Parker GJ, Symms M, Boulby P, Wheeler-Kingshott CA, Salek-Haddadi A, Barker GJ, Duncan JS (2003) Combined functional MRI and tractography to demonstrate the connectivity of the human primary motor cortex in vivo. Neuroimage 19: 1349–1360

Hahn E (1950) Spin Echoes. Physics Review 80: 580–594

Hasan KM, Basser PJ, Parker DL, Alexander AL (2001a) Analytical computation of the eigenvalues and eigenvectors in DT-MRI. Journal of Magnetic Resonance 152: 41–47

Hasan KM, Parker DL, Alexander AL (2001b) Comparison of gradient encoding schemes for diffusion-tensor MRI. Journal of Magnetic Resonance Imaging 13: 769–780

Haselgrove JC, Moore JR (1996) Correction for distortion of echo-planar images used to calculate the apparent diffusion coefficient. Magnetic Resonance in Medicine 36: 960–964

Heiervang E, Behrens TE, Mackay CE, Robson MD, Johansen-Berg H (2006) Between session reproducibility and between subject variability of diffusion MR and tractography measures. Neuroimage 33: 867–877

Henkelman RM, Huang X, Xiang QS, Stanisz GJ, Swanson SD, Bronskill MJ (1993) Quantitative interpretation of magnetization transfer. Magnetic Resonance in Medicine 29: 759–766

Henkelman RM, Stanisz GJ, Graham SJ (2001) Magnetization transfer in MRI: a review. NMR in Biomedicine 14: 57–64

Henry RG, Berman JI, Nagarajan SS, Mukherjee P, Berger MS (2004) Subcortical pathways serving cortical language sites: initial experience with diffusion tensor imaging fiber tracking combined with intraoperative language mapping. Neuroimage 21: 616–622

Hickman SJ, Toosy AT, Jones SJ, Altmann DR, Miszkiel KA, MacManus DG, Barker GJ, Plant GT, Thompson AJ, Miller DH (2004) Serial magnetization transfer imaging in acute optic neuritis. Brain 127: 692–700

Holodny AI, Schwartz TH, Ollenschleger M, Liu WC, Schulder M (2001) Tumor involvement of the corticospinal tract: diffusion magnetic resonance tractography with intraoperative correlation. Journal of Neurosurgery 95: 1082

Horsfield MA, Barker GJ, Barkhof F, Miller DH, Thompson AJ, Filippi M (2003) Guidelines for using quantitative magnetization transfer magnetic resonance imaging for monitoring treatment of multiple sclerosis. Journal of Magnetic Resonance Imaging 17: 389–397

Horwitz B, Duara R, Rapoport SI (1984) Intercorrelations of glucose metabolic rates between brain regions: application to healthy males in a state of reduced sensory input. Journal of Cerebral Blood Flow and Metabolism 4: 484–499

Horwitz B, Tagamets MA, McIntosh AR (1999) Neural modeling, functional brain imaging, and cognition. Trends in Cognitive Sciences 3: 91–98

Jacob S, Finsterbusch J, Weishaupt JH, Khorram-Sefat D, Frahm J, Ehrenreich H (2003) Diffusion tensor imaging for long-term follow-up of corticospinal tract degeneration in amyotrophic lateral sclerosis. Neuroradiology 45: 598–600

Jellison BJ, Field AS, Medow J, Lazar M, Salamat MS, Alexander AL (2004) Diffusion tensor imaging of cerebral white matter: a pictorial review of physics, fiber tract anatomy, and tumor imaging patterns. AJNR: American Journal of Neuroradiology 25: 356–369

Jernigan TL, Archibald SL, Berhow MT, Sowell ER, Foster DS, Hesselink JR (1991) Cerebral structure on MRI, Part I: Localization of age-related changes. Biological Psychiatry 29: 55–67

Jezzard P, Balaban RS (1995) Correction for geometric distortion in echo planar images from B0 field variations. Magnetic Resonance in Medicine 34: 65–73

Johansen-Berg H, Behrens TE, Robson MD, Drobnjak I, Rushworth MF, Brady JM, Smith SM, Higham DJ, Matthews PM (2004) Changes in connectivity profiles define functionally distinct regions in human medial frontal cortex. Proceedings of the National Academy of Sciences of the United States of America 101: 13335–13340

Johansen-Berg H, Behrens TE, Sillery E, Ciccarelli O, Thompson AJ, Smith SM, Matthews PM (2005) Functional-anatomical validation and individual variation of diffusion tractography-based segmentation of the human thalamus. Cerebral Cortex 15: 31–39

Jones CK, Xiang QS, Whittall KP, MacKay AL (2004) Linear combination of multiecho data: short T2 component selection. Magnetic Resonance in Medicine 51: 495–502

Jones DK (2003) Determining and Visualizing Uncertainty in Estimates of Fiber Orientation From Diffusion Tensor MRI. Magnetic Resonance in Medicine 49: 7–12

Jones DK (2004) The effect of gradient sampling schemes on measures derived from diffusion tensor MRI: a Monte Carlo study. Magnetic Resonance in Medicine 51: 807–815

Jones DK, Catani M, Pierpaoli C, Reeves SJ, Shergill SS, O'Sullivan M, Golesworthy P, McGuire P, Horsfield MA, Simmons A, Williams SC, Howard RJ (2006) Age effects on diffusion tensor magnetic resonance imaging tractography measures of frontal cortex connections in schizophrenia. Human Brain Mapping 27: 230–238

Jones DK, Catani M, Pierpaoli C, Reeves SJ, Shergill SS, O'Sullivan M, Maguire P, Horsfield MA, Simmons A, Williams SC, Howard RJ (2005a) A diffusion tensor magnetic resonance imaging study of frontal cortex connections in very-late-onset schizophrenia-like psychosis. American Journal of Geriatric Psychiatry 13: 1092–1099

Jones DK, Griffin LD, Alexander DC, Catani M, Horsfield MA, Howard R, Williams SC (2002a) Spatial normalization and averaging of diffusion tensor MRI data sets. Neuroimage 17: 592–617

Jones DK, Horsfield MA, Simmons A (1999) Optimal strategies for measuring diffusion in anisotropic systems by magnetic resonance imaging. Magnetic Resonance in Medicine 42: 515–525

Jones DK, Symms MR, Cercignani M, Howard RJ (2005b) The effect of filter size on VBM analyses of DT-MRI data. Neuroimage 26: 546–554

Jones DK, Travis AR, Eden G, Pierpaoli C, Basser PJ (2005c) PASTA: pointwise assessment of streamline tractography attributes. Magnetic Resonance in Medicine 53: 1462–1467

Jones DK, Williams SC, Gasston D, Horsfield MA, Simmons A, Howard R (2002b) Isotropic resolution diffusion tensor imaging with whole brain acquisition in a clinically acceptable time. Human Brain Mapping 15: 216–230

Kabani NJ, Sled JG, Chertkow H (2002a) Magnetization transfer ratio in mild cognitive impairment and dementia of Alzheimer's type. Neuroimage 15: 604–610

Kabani NJ, Sled JG, Shuper A, Chertkow H (2002b) Regional magnetization transfer ratio changes in mild cognitive impairment. Magnetic Resonance in Medicine 47: 143–148

Kalus P, Slotboom J, Gallinat J, Wiest R, Ozdoba C, Federspiel A, Strik WK, Buri C, Schroth G, Kiefer C (2005) The amygdala in schizophrenia: a trimodal magnetic resonance imaging study. Neuroscience Letters 375: 151–156

Kanaan RA, Shergill SS, Barker GJ, Catani M, Ng VW, Howard R, McGuire PK, Jones DK (2006) Tract-specific anisotropy measurements in diffusion tensor imaging. Psychiatry Research 146: 73–82

Kiebel SJ, Poline JB, Friston KJ, Holmes AP, Worsley KJ (1999) Robust smoothness estimation in statistical parametric maps using standardized residuals from the general linear model. Neuroimage 10: 756–766

Kiefer C, Slotboom J, Buri C, Gralla J, Remonda L, Dierks T, Strik WK, Schroth G, Kalus P (2004) Differentiating hippocampal subregions by means of quantitative magnetization transfer and relaxometry: preliminary results. Neuroimage 23: 1093–1099

Kinoshita M, Yamada K, Hashimoto N, Kato A, Izumoto S, Baba T, Maruno M, Nishimura T, Yoshimine T (2005) Fiber-tracking does not accurately estimate size of fiber bundle in pathological condition: initial neurosurgical experience using neuronavigation and subcortical white matter stimulation. Neuroimage 25: 424–429

Kubicki M, Park H, Westin CF, Nestor PG, Mulkern RV, Maier SE, Niznikiewicz M, Connor EE, Levitt JJ, Frumin M, Kikinis R, Jolesz FA, McCarley RW, Shenton ME (2005) DTI and MTR abnormalities in schizophrenia: analysis of white matter integrity.

Kumar A, Gupta RC, Albert Thomas M, Alger J, Wyckoff N, Hwang S (2004) Biophysical changes in normal-appearing white matter and subcortical nuclei in late-life major depression detected using magnetization transfer. Psychiatry Research 130: 131–140

Laule C, Vavasour IM, Moore GR, Oger J, Li DK, Paty DW, MacKay AL (2004) Water content and myelin water fraction in multiple sclerosis. A T2 relaxation study. Journal of Neurology 251: 284–293

Lazar M, Alexander AL (2002) White matter tractography using random vector (RAVE) perturbation. Proceedings of 10th Annual Meeting of the ISMRM, Honolulu, Hawaii: 539

Lazar M, Alexander AL (2005) Bootstrap white matter tractography (BOOT-TRAC). Neuroimage 24: 524–532

Lazar M, Alexander AL, Thottakara P, Badie B, Field AS (2006) White matter reorganization after surgical resection of brain tumors and vascular malformations. AJNR: American Journal of Neuroradiology: in press

Lazar M, Weinstein DM, Tsuruda JS, Hasan KM, Arfanakis K, Meyerand ME, Badie B, Rowley HA, Haughton V, Field A, Alexander AL (2003) White matter tractography using diffusion tensor deflection. Human Brain Mapping 18: 306–321

Le Bihan D (1990) Diffusion/perfusion MR imaging of the brain: from structure to function. Radiology 177: 328–329

Lim KO, Hedehus M, Moseley M, de Crespigny A, Sullivan EV, Pfefferbaum A (1999) Compromised white matter tract integrity in schizophrenia inferred from diffusion tensor imaging. Archives of General Psychiatry 56: 367–374

Lin X, Tench CR, Morgan PS, Niepel G, Constantinescu CS (2005) 'Importance sampling' in MS: use of diffusion tensor tractography to quantify pathology related to specific impairment. Journal of the Neurological Sciences 237: 13–19

Liu C, Bammer R, Acar B, Moseley ME (2004) Characterizing non-Gaussian diffusion by using generalized diffusion tensors. Magnetic Resonance in Medicine 51: 924–937

MacKay A, Laule C, Vavasour I, Bjarnason T, Kolind S, Madler B (2006) Insights into brain microstructure from the T2 distribution. Magnetic resonance imaging. 24: 515–525

MacKay A, Whittall K, Adler J, Li D, Paty D, Graeb D (1994) In vivo visualization of myelin water in brain by magnetic resonance. Magnetic Resonance in Medicine 31: 673–677

Madden DJ, Whiting WL, Huettel SA, White LE, MacFall JR, Provenzale JM (2004) Diffusion tensor imaging of adult age differences in cerebral white matter: relation to response time. Neuroimage 21: 1174–1181

Maier SE, Vajapeyam S, Mamata H, Westin CF, Jolesz FA, Mulkern RV (2004) Biexponential diffusion tensor analysis of human brain diffusion data. Magnetic Resonance in Medicine 51: 321–330

Makris N, Worth AJ, Sorensen AG, Papadimitriou GM, Wu O, Reese TG, Wedeen VJ, Davis TL, Stakes JW, Caviness VS, Kaplan E, Rosen BR, Pandya DN, Kennedy DN (1997) Morphometry of in vivo human white matter association pathways with diffusion-weighted magnetic resonance imaging. Annals of Neurology 42: 951–962

Mansfield P (1984) Real-time echo-planar imaging by NMR. British Medical Bulletin 40: 187–190

Martin, Kikinis R, Zuerrer M, Boesch C, Briner J, Kewity G, Kaelin P (1988) Developmental stages of human brain: an MR study. Journal of Computer Assisted Tomography 12: 917–922

McIntosh AR (2000) Towards a network theory of cognition. Neural Networks 13: 861–870

Menon RS, Allen PS (1991) Application of continuous relaxation time distributions to the fitting of data from model systems and excised tissue. Magnetic Resonance in Medicine 20: 214–227

Miot-Noirault E, Barantin L, Akoka S, Le Pape A (1997) T2 relaxation time as a marker of brain myelination: experimental MR study in two neonatal animal models. Journal of Neuroscience Methods 72: 5–14

Miot E, Hoffschir D, Poncy JL, Masse R, Le Pape A, Akoka S (1995) Magnetic resonance imaging in vivo monitoring of T2 relaxation time: quantitative assessment of primate brain maturation. Journal of Medical Primatology 24: 87–93

Mori S, Crain BJ, Chacko VP, van Zijl PCM (1999) Three-dimensional tracking of axonal projections in the brain by magnetic resonance imaging. Annals of Neurology 45: 265–269

Moseley ME, Cohen Y, Kucharczyk J, Mintorovitch J, Asgari HS, Wendland MF, Tsuruda J, Norman D (1990) Diffusion-weighted MR imaging of anisotropic water diffusion in cat central nervous system. Radiology 176: 439–445

Mulkern RV, Gudbjartsson H, Westin CF, Zengingonul HP, Gartner W, Guttmann CR, Robertson RL, Kyriakos W, Schwartz R, Holtzman D, Jolesz FA, Maier SE (1999) Multi-component apparent diffusion coefficients in human brain. NMR in Biomedicine 12: 51–62

Neil J, Miller J, Mukherjee P, Huppi PS (2002) Diffusion tensor imaging of normal and injured developing human brain - a technical review. NMR in Biomedicine 15: 543–552

Niendorf T, Dijkhuizen RM, Norris DG, van Lookeren Campagne M, Nicolay K (1996) Biexponential diffusion attenuation in various states of brain tissue: implications for diffusion-weighted imaging. Magnetic Resonance in Medicine 36: 847–857

Oh J, Han ET, Pelletier D, Nelson SJ (2006) Measurement of in vivo multi-component T2 relaxation times for brain tissue using multi-slice T2 prep at 1.5 and 3 T. Magnetic Resonance Imaging 24: 33–43

Olesen PJ, Nagy Z, Westerberg H, Klingberg T (2003) Combined analysis of DTI and fMRI data reveals a joint maturation of white and grey matter in a fronto-parietal network. Cognitive Brain Research 18: 48–57

Ozarslan E, Mareci TH (2003) Generalized diffusion tensor imaging and analytical relationships between diffusion tensor imaging and high angular resolution diffusion imaging. Magnetic Resonance in Medicine 50: 955–965

Pajevic S, Pierpaoli C (1999) Color schemes to represent the orientation of anisotropic tissues from diffusion tensor data: application to white matter fiber tract mapping in the human brain. Magnetic Resonance in Medicine 42: 526–540

Papadakis NG, Martin KM, Mustafa MH, Wilkinson ID, Griffiths PD, Huang CL, Woodruff PW (2002) Study of the effect of CSF suppression on white matter diffusion anisotropy mapping of healthy human brain. Magnetic Resonance in Medicine 48: 394–398

Papadakis NG, Xing D, Huang CL, Hall LD, Carpenter TA (1999) A comparative study of acquisition schemes for diffusion tensor imaging using MRI. Journal of Magnetic Resonance 137: 67–82

Park H-J, Kubicki M, Shenton ME, Guimond A, McCarley RW, Maier SE, Kikinis R, Jolesz FA, Westin CF (2003) Spatial normalization of diffusion tensor MRI using multiple channels. Neuroimage 20: 1995–2009

Parker GJ, Haroon HA, Wheeler-Kingshott CA (2003) A framework for a streamline-based probabilistic index of connectivity (PICo) using a structural interpretation of MRI diffusion measurements. Journal of Magnetic Resonance Imaging 18: 242–254

Parker GJ, Stephan KE, Barker GJ, Rowe JB, MacManus DG, Wheeler-Kingshott CA, Ciccarelli O, Passingham RE, Spinks RL, Lemon RN, Turner R (2002) Initial demonstration of in vivo tracing of axonal projections in the macaque brain and comparison with the human brain using diffusion tensor imaging and fast marching tractography. Neuroimage 15: 797–809

Paus T, Collins DL, Evans AC, Leonard G, Pike B, Zijdenbos A (2001) Maturation of white matter in the human brain: a review of magnetic resonance studies. Brain Research Bulletin 54: 255–266

Penny WD, Stephan KE, Mechelli A, Friston KJ (2004) Modelling functional integration: a comparison of structural equation and dynamic causal models. Neuroimage 23 Suppl 1: S264–274

Pfefferbaum A, Adalsteinsson E, Sullivan EV (2005) Frontal circuitry degradation marks healthy adult aging: Evidence from diffusion tensor imaging. Neuroimage 26: 891–899

Pierpaoli C, Basser PJ (1996) Toward a quantitative assessment of diffusion anisotropy. Magnetic Resonance in Medicine 36: 893–906

Pipe JG, Farthing VG, Forbes KP (2002) Multishot diffusion-weighted FSE using PROPELLER MRI.[erratum appears in Magn Reson Med 2002 Mar;47(3):621]. Magnetic Resonance in Medicine 47: 42–52

Pomara N, Crandall DT, Choi SJ, Johnson G, Lim KO (2001) White matter abnormalities in HIV-1 infection: a diffusion tensor imaging study. Psychiatry Research 106: 15–24

Poon CS, Henkelman RM (1992) Practical T2 quantitation for clinical applications. Journal of Magnetic Resonance Imaging 2: 541–553

Poon CS, Henkelman RM (1995) Robust refocusing pulses of limited power. Journal of Magnetic Resonance 116: 161–180

Prayer D, Prayer L (2003) Diffusion-weighted magnetic resonance imaging of cerebral white matter development. European Journal of Radiology 45: 235–243

Pruessmann KP, Weiger M, Scheidegger MB, Boesiger P (1999) SENSE: sensitivity encoding for fast MRI. Magnetic Resonance in Medicine 42: 952–962

Rademacher J, Engelbrecht V, Burgel U, Freund H, Zilles K (1999) Measuring in vivo myelination of human white matter fiber tracts with magnetization transfer MR. Neuroimage 9: 393–406

Ragin AB, Storey P, Cohen BA, Epstein LG, Edelman RR (2004) Whole brain diffusion tensor imaging in HIV-associated cognitive impairment. AJNR: American Journal of Neuroradiology 25: 195–200

Ramnani N, Behrens TE, Penny W, Matthews PM (2004) New approaches for exploring anatomical and functional connectivity in the human brain. Biological Psychiatry 56: 613–619

Reese TG, Heid O, Weisskoff RM, Wedeen VJ (2003) Reduction of eddy-current-induced distortion in diffusion MRI using a twice-refocused spin echo. Magnetic Resonance in Medicine 49: 177–182

Rocca MA, Agosta F, Martinelli V, Falini A, Comi G, Filippi M (2005) The level of spinal cord involvement influences the pattern of movement-associated cortical recruitment in patients with isolated myelitis. Neuroimage

Rohde GK, Barnett AS, Basser PJ, Marenco S, Pierpaoli C (2004) Comprehensive approach for correction of motion and distortion in diffusion-weighted MRI. Magnetic Resonance in Medicine 51: 103–114

Rohde GK, Barnett AS, Basser PJ, Pierpaoli C (2005) Estimating intensity variance due to noise in registered images: applications to diffusion tensor MRI. Neuroimage 26: 673–684

Ronen I, Ugurbil K, Kim DS (2005) How does DWI correlate with white matter structures? Magnetic Resonance in Medicine 54: 317–323

Ropele S, Filippi M, Valsasina P, Korteweg T, Barkhof F, Tofts PS, Samson R, Miller DH, Fazekas F (2005) Assessment and correction of B1-induced errors in magnetization transfer ratio measurements. Magnetic Resonance in Medicine 53: 134–140

Rovaris M, Iannucci G, Falautano M, Possa F, Martinelli V, Comi G, Filippi M (2002) Cognitive dysfunction in patients with mildly disabling relapsing-remitting multiple sclerosis: an exploratory study with diffusion tensor MR imaging. Journal of the Neurological Sciences 195: 103–109

Rushworth MF, Behrens TE, Johansen-Berg H (2005) Connection Patterns Distinguish 3 Regions of Human Parietal Cortex. Cerebral Cortex: epub ahead of print

Salat DH, Tuch DS, Greve DN, van der Kouwe AJ, Hevelone ND, Zaleta AK, Rosen BR, Fischl B, Corkin S, Rosas HD, Dale AM (2005) Age-related alterations in white matter microstructure measured by diffusion tensor imaging. Neurobiology of Aging 26: 1215–1227

Salmond CH, Menon DK, Chatfield DA, Williams GB, Pena A, Sahakian BJ, Pickard JD (2006) Diffusion tensor imaging in chronic head injury survivors: correlations with learning and memory indices. Neuroimage 29: 117–124

Salonen O, Autti T, Raininko R, Ylikoski A, Erkinjuntti T (1997) MRI of the brain in neurologically healthy middle-aged and elderly individuals. Neuroradiology 39: 537–545

Santyr GE (1993) Magnetization transfer effects in multislice MR imaging. Magnetic Resonance Imaging 11: 521–532

Shimony JS, McKinstry RC, Akbudak E, Aronovitz JA, Snyder AZ, Lori NF, Cull TS, Conturo TE (1999) Quantitative diffusion-tensor anisotropy brain MR imaging: normative human data and anatomic analysis. Radiology 212: 770–784

Shrager RI, Basser PJ (1998) Anisotropically weighted MRI. Magnetic Resonance in Medicine 40: 160–165

Sie LT, van der Knaap MS, van Wezel-Meijler G, Valk J (1997) MRI assessment of myelination of motor and sensory pathways in the brain of preterm and term-born infants. Neuropediatrics 28: 97–105

Skare S, Andersson JL (2001) On the effects of gating in diffusion imaging of the brain using single shot EPI. Magnetic Resonance Imaging 19: 1125–1128

Skare S, Li T-Q, Nordell B, Ingvar M (2000) Noise considerations in the determination of diffusion tensor anisotropy. Magnetic Resonance Imaging 18: 659–669

Sled JG, Pike B (2000) Correction for B1 and B0 variations in quantitative T2 measurements using MRI. Magnetic Resonance in Medicine 43: 589–593

Sled JG, Pike GB (2001) Quantitative imaging of magnetization transfer exchange and relaxation properties in vivo using MRI. Magnetic Resonance in Medicine 46: 923–931

Smith SM, Jenkinson M, Johansen-Berg H, Rueckert D, Nichols TE, Mackay C, Watkins KE, Ciccarelli O, Cader MZ, M. MP, E.J. B (2006) Tract-Based Spatial Statistics: Voxelwise Analysis of Multi-Subject Diffusion Data. Neuroimage: under review

Snook L, Paulson LA, Roy D, Phillips L, Beaulieu C (2005) Diffusion tensor imaging of neurodevelopment in children and young adults. Neuroimage 26: 1164–1173

Song SK, Sun SW, Ramsbottom MJ, Chang C, Russell J, Cross AH (2002) Dysmyelination revealed through MRI as increased radial (but unchanged axial) diffusion of water. Neuroimage 17: 1429–1436

Song SK, Yoshino J, Le TQ, Lin SJ, Sun SW, Cross AH, Armstrong RC (2005) Demyelination increases radial diffusivity in corpus callosum of mouse brain. Neuroimage 26: 132–140

Stanisz GJ, Henkelman RM (1998) Diffusional anisotropy of T2 components in bovine optic nerve. Magnetic Resonance in Medicine 40: 405–410

Stanisz GJ, Kecojevic A, Bronskill MJ, Henkelman RM (1999) Characterizing white matter with magnetization transfer and T. Magnetic Resonance in Medicine 42: 1128–1136

Stanisz GJ, Webb S, Munro CA, Pun T, Midha R (2004) MR properties of excised neural tissue following experimentally induced inflammation. Magnetic Resonance in Medicine 51: 473–479

Steen RG, Ogg RJ, Reddick WE, Kingsley PB (1997) Age-related changes in the pediatric brain: quantitative MR evidence of maturational changes during adolescence. AJNR: American Journal of Neuroradiology 18: 819–828

Stejskal E, Tanner J (1965) Spin diffusion measurements: Spin echoes in the presence of a time-dependent field gradient. Journal of Chemical Physics 42: 288–292

Stephan KE (2004) On the role of general system theory for functional neuroimaging. Journal of Anatomy 205: 443–470

Stephan KE, Harrison LM, Penny WD, Friston KJ (2004) Biophysical models of fMRI responses. Current Opinion in Neurobiology 14: 629–635

Stephan KE, Penny WD, Marshall JC, Fink GR, Friston KJ (2005) Investigating the functional role of callosal connections with dynamic causal models. Annals of the New York Academy of Science 1064: 16–36

Stieltjes B, Kaufmann WE, van Zijl PC, Fredericksen K, Pearlson GD, Solaiyappan M, Mori S (2001) Diffusion tensor imaging and axonal tracking in the human brainstem. Neuroimage 14: 723–735

Szeszko PR, Ardekani BA, Ashtari M, Malhotra AK, Robinson DG, Bilder RM, Lim KO (2005) White matter abnormalities in obsessive-compulsive disorder: a diffusion tensor imaging study. Archives of General Psychiatry 62: 782–790

Thottakara P, Lazar M, Johnson SC, Alexander AL (2006) Application of Brodmann's area templates for ROI selection in white matter tractography studies. Neuroimage 29: 868–878

Toosy AT, Ciccarelli O, Parker GJ, Wheeler-Kingshott CA, Miller DH, Thompson AJ (2004) Characterizing function-structure relationships in the human visual system with functional MRI and diffusion tensor imaging. Neuroimage 21: 1452–1463

Toosy AT, Werring DJ, Orrell RW, Howard RS, King MD, Barker GJ, Miller DH, Thompson AJ (2003) Diffusion tensor imaging detects corticospinal tract involvement at multiple levels in amyotrophic lateral sclerosis. Journal of Neurology, Neurosurgery & Psychiatry 74: 1250–1257

Townsend TN, Bernasconi N, Pike GB, Bernasconi A (2004) Quantitative analysis of temporal lobe white matter T2 relaxation time in temporal lobe epilepsy. Neuroimage 23: 318–324

Tozer D, Ramani A, Barker GJ, Davies GR, Miller DH, Tofts PS (2003) Quantitative magnetization transfer mapping of bound protons in multiple sclerosis. Magnetic Resonance in Medicine 50: 83–91

Tozer DJ, Davies GR, Altmann DR, Miller DH, Tofts PS (2005) Correlation of apparent myelin measures obtained in multiple sclerosis patients and controls from magnetization transfer and multicompartmental T2 analysis. Magnetic Resonance in Medicine 53: 1415–1422

Tuch DS (2004) Q-ball imaging. Magnetic Resonance in Medicine 52: 1358–1372

Tuch DS, Salat DH, Wisco JJ, Zaleta AK, Hevelone ND, Rosas HD (2005) Choice reaction time performance correlates with diffusion anisotropy in white matter pathways supporting visuospatial attention. Proceedings of the National Academy of Sciences of the United States of America 102: 12212–12217

Tuch DS, Wedeen VJ, Dale AM, George JS, Belliveau JW (2001) Conductivity tensor mapping of the human brain using diffusion tensor MRI. Proceedings of the National Academy of Sciences of the United States of America 98: 11697–11701

Turner R, Le Bihan D, Maier J, Vavrek R, Hedges LK, Pekar J (1990) Echo-planar imaging of intravoxel incoherent motion. Radiology 177: 407–414

Ulug AM, van Zijl PC (1999) Orientation-independent diffusion imaging without tensor diagonalization: anisotropy definitions based on physical attributes of the diffusion ellipsoid. Journal of Magnetic Resonance Imaging 9: 804–813

Vaithianathar L, Tench CR, Morgan PS, Wilson M, Blumhardt LD (2002) T1 relaxation time mapping of white matter tracts in multiple sclerosis defined by diffusion tensor imaging. Journal of Neurology 249: 1272–1278

van Buchem MA, Steens SC, Vrooman HA, Zwinderman AH, McGowan JC, Rassek M, Engelbrecht V (2001) Global estimation of myelination in the developing brain on the basis of magnetization transfer imaging: a preliminary study. AJNR: American Journal of Neuroradiology 22: 762–766

Vavasour IM, Whittall KP, MacKay AL, Li DK, Vorobeychik G, Paty DW (1998) A comparison between magnetization transfer ratios and myelin water percentages in normals and multiple sclerosis patients. Magnetic Resonance in Medicine 40: 763–768

Vidarsson L, Conolly SM, Lim KO, Gold GE, Pauly JM (2005) Echo time optimization for linear combination myelin imaging. Magnetic Resonance in Medicine 53: 398–407

Wakana S, Jiang H, Nagae-Poetscher LM, van Zijl PC, Mori S (2004) Fiber tract-based atlas of human white matter anatomy. Radiology 230: 77–87

Webb S, Munro CA, Midha R, Stanisz GJ (2003) Is multicomponent T2 a good measure of myelin content in peripheral nerve? Magnetic Resonance in Medicine 49: 638–645

Wedeen VJ, Hagmann P, Tseng WY, Reese TG, Weisskoff RM (2005) Mapping complex tissue architecture with diffusion spectrum magnetic resonance imaging. Magnetic Resonance in Medicine 54: 1377–1386

Werring DJ, Clark CA, Barker GJ, Miller DH, Parker GJ, Brammer MJ, Bullmore ET, Giampietro VP, Thompson AJ (1998) The structural and functional mechanisms of motor recovery: complementary use of diffusion tensor and functional magnetic resonance imaging in a traumatic injury of the internal capsule. Journal of Neurology, Neurosurgery & Psychiatry 65: 863–869

Westin CF, Maier SE, Mamata H, Nabavi A, Jolesz FA, Kikinis R (2002) Processing and visualization for diffusion tensor MRI. Medical Image Analysis 6: 93–108

Whittall KP, MacKay AL, Graeb DA, Nugent RA, Li DK, Paty DW (1997) In vivo measurement of T2 distributions and water contents in normal human brain. Magnetic Resonance in Medicine 37: 34–43

Whittall KP, MacKay AL, Li DK, Vavasour IM, Jones CK, Paty DW (2002) Normal-appearing white matter in multiple sclerosis has heterogeneous, diffusely prolonged T(2). Magnetic Resonance in Medicine 47: 403–408

Whittall KP, MacKay AL, Li DKB (1999) Are mono-exponential fits to a few echoes sufficient to determine T2 relaxation for in-vivo human brain? Magnetic Resonance in Medicine 41: 1255–1257

Witwer BP, Moftakhar R, Hasan KM, Deshmukh P, Haughton V, Field A, Arfanakis K, Noyes J, Moritz CH, Meyerand ME, Rowley HA, Alexander AL, Badie B (2002) Diffusion-tensor imaging of white matter tracts in patients with cerebral neoplasm. Journal of Neurosurgery 97: 568–575

Wu YC, Alexander AL (2005) Hybrid diffusion imaging for complex diffusion characterization. Proceedings of the 13th ISMRM Scientific Meeting: 578

Wu YC, Field AS, Chung MK, Badie B, Alexander AL (2004) Quantitative analysis of diffusion tensor orientation: theoretical framework. Magnetic Resonance in Medicine 52: 1146–1155

Xu D, Mori S, Shen D, van Zijl PC, Davatzikos C (2003) Spatial normalization of diffusion tensor fields. Magnetic Resonance in Medicine 50: 175–182

Yarnykh VL (2002) Pulsed Z-spectroscopic imaging of cross-relaxation parameters in tissues for human MRI: theory and clinical applications. Magnetic Resonance in Medicine 47: 929–939

Yarnykh VL, Yuan C (2004) Cross-relaxation imaging reveals detailed anatomy of white matter fiber tracts in the human brain. Neuroimage 23: 409–424

Zhang Y, Wehrli FW (2004) Reference-scan-free method for automated correction of Nyquist ghost artifacts in echoplanar brain images. Magnetic Resonance in Medicine 51: 621–624